REPORT DOCUMENTATION PAGE

Form Approved
OMB NO. 0704-0188

1. AGENCY USE ONLY (Leave Blank)	2. REPORT DATE	3. REPORT TYPE AND DATES COVERED
	August 31, 2007	Interim Progress Report, August 01, 2006 to July 31, 2007

4. TITLE AND SUBTITLE
Nano Engineered Energetic Materials (NEEM)

5. FUNDING NUMBERS
W911NF-04-1-0178

6. AUTHOR(S)
David Allara, Dana Dlott, Greg Girolami, Rajiv Kalia, Kenneth Kuo, Aiichiro Nakano, Ralph Nuzzo, Priya Vashishta, Vigor Yang, and Richard Yetter

7. PERFORMING ORGANIZATION NAME(S) AND ADDRESS(ES)
The Pennsylvania State University, University Park, PA
The University of Illinois at Urbana-Champaign, Urbana, IL
University of Southern California, Los Angeles, CA

8. PERFORMING ORGANIZATION REPORT NUMBER

9. SPONSORING / MONITORING AGENCY NAME(S) AND ADDRESS(ES)

U. S. Army Research Office
P.O. Box 12211
Research Triangle Park, NC 27709-2211

10. SPONSORING / MONITORING AGENCY REPORT NUMBER

11. SUPPLEMENTARY NOTES
The views, opinions and/or findings contained in this report are those of the author(s) and should not be construed as an official Department of the Army position, policy or decision, unless so designated by other documentation.

12 a. DISTRIBUTION / AVAILABILITY STATEMENT

Approved for public release; distribution unlimited.

12 b. DISTRIBUTION CODE

13. ABSTRACT (Maximum 200 words)

The **Nano Engineered Energetic Materials** (**NEEM**) MURI program is exploring new methodologies for development of energetic material formulations with control of all constituents over a wide range of length scales from 1 nm to 1 mm and larger. New methods employing the latest techniques in molecular self-assembly and supramolecular chemistry for synthesizing and assembling nano-structured energetic materials are under study. The synthetic efforts are guided by theoretical calculations and dynamic performance testing methodologies that also operate on all length scales. During the past year, boron nanoparticles (>97%B) with a size range of 10-50nm were fabricated by pyrolysis of decaborane. The nB particles are easily suspended in organic solvents and are currently being examined for their combustion behavior. A new method for formation of stabilized Al nanowires in a hydrocarbon SAM was developed. The nanofilaments are believed to have diameters of 1-3 Al atoms with lengths of ~2nm. Supercritical processing of nano RDX with particle diameters ranging from 93-509 nm was demonstrated. The RDX particle recovery was greater than 90% of the initial material. Electrostatic self-assembly was used to form microspheres consisting of a nAl/nCuO thermite. Large multiscale simulations with quantum-mechanical and molecular dynamics calculations were used to study the shock compression of self-assembled monolayers, the flash heating of an alumina nanoparticle, and the melting of a nAl particle. Dynamic performance of NEEMs containing nAl particles were characterized using ultrafast IR and emission spectroscopy and flash laser heating and laser-generated shock waves. Combustion of nAl/nCuO thermites over a wide pressure range and particle size distribution were examined along with mixtures of $nAl/H_2O/H_2O_2$ and nAl/CH_3NO_2.

14. SUBJECT TERMS
Energetic materials, nanotechnology, nano aluminum, nano boron, self-assembly, supercritical fluid processing, atomistic and molecular dynamics modeling, ultra-fast molecular spectroscopy, combustion

15. NUMBER OF PAGES
33

16. PRICE CODE

17. SECURITY CLASSIFICATION OR REPORT	18. SECURITY CLASSIFICATION ON THIS PAGE	19. SECURITY CLASSIFICATION OF ABSTRACT	20. LIMITATION OF ABSTRACT
UNCLASSIFIED	**UNCLASSIFIED**	**UNCLASSIFIED**	**UL**

REPORT DOCUMENTATION PAGE (SF298)
(Continuation Sheet)

Table of Contents

Introduction

Novel energetic materials science and nanotechnology are recognized as critical enablers in support of a changing armed-force structure that will require new and advanced explosives and propellants.

Nanotechnology is a promising method of making new munitions, but the processes which determine the performance of nanotechnology munitions lie in a realm in between the better-known engineering models of bulk materials and chemical reaction dynamics of molecules, and are not yet well understood. Nanotechnology also offers the possibility of an unprecedented level of control over the structure of a munition on length scales from nanometers to meters. However, a firm understanding of the relationships between nanostructure and performance and how to design optimal devices for specified tasks are not yet known.

Two critical observations relevant to the future development of nanostructured energetic materials can therefore be made: *(1) self-assembly and supramolecular chemistry of the fuel and oxidizer elements of energetic materials has lagged far behind other chemistries, and (2) there is no fundamental understanding of exactly what supramolecular structures provide desirable performance, mechanical, and hazard characteristics.* With advancements on these two fronts, it is conceivable that macroscale formulations of energetic materials could be designed to preserve the intrinsic nanoscale structure of individual components, thus achieving the true potential of nanoscale energetic materials.

The present MURI program on **Nano Engineered Energetic Materials** (**NEEM**) is exploring new methods employing the latest techniques in molecular self-assembly and supramolecular control for synthesizing and assembling nano-structured energetic materials. The synthetic efforts of the program are being guided by state-of-the-art theoretical calculations and by advanced dynamic performance testing methodologies that also operate on all length scales.

Objectives and Approach

Two overall objectives of the NEEM MURI program are:

- The development of new methodologies for synthesis and assembly of nano-engineered energetic materials (NEEMs), which will also provide concurrent improvement in performance and managed energy release while providing reduced sensitivity and ease of processing and handling.
- The fundamental understanding of the relationship between the structures of NEEMs and their reactive and mechanical behavior, particularly with regard to sensitivity, ignition, burning characteristics, mechanical properties, and optimum loading density, thus enabling design optimization of NEEMs.

To accomplish these objectives, the program makes use of a combination of novel nanotechnology fabrication techniques, state-of-the-art theoretical modeling techniques that can interrogate events occurring from the atomistic/molecular scale through the mesoscale to the macroscale, and experimental diagnostic techniques that can capture the reactive dynamics at femtosecond timescales to those that evaluate overall combustion performance.

Organization

Scientists and engineers from three universities are included in the program: the Pennsylvania State University (PSU), the University of Illinois at Urbana-Champaign (UIUC), and the University of Southern California (USC). The team consists of chemists with expertise at the juncture of organic and inorganic chemistry who were among the original developers of molecular self-assembly (**Allara, Nuzzo, Girolami**), mechanical engineers with expertise in the formulation of real, practical propellants (**Kuo, Yetter**), theoreticians who use teraflop supercomputers to understand the chemical reactions of fuels and oxidizers from the level of individual atoms (**Vashishta**) to the macroscale (**Nakano, Kalia, Yang**), a physical chemist who pioneered the use of ultrafast laser spectroscopy to study initiation of energetic materials (**Dlott**), and mechanical engineers with expertise in the experimental and theoretical characterization of real-world performance parameters of energetic materials (**Kuo, Yetter, Yang**).

The overall research program is divided into three major inter-related areas: (1) synthesis, self-assembly and supramolecular chemistry of NEEMs, (2) theoretical modeling of the physiochemical processes and mechanical behavior of NEEMs, and (3) experimental characterization of the reaction dynamics of NEEMs (**Fig. 1**).

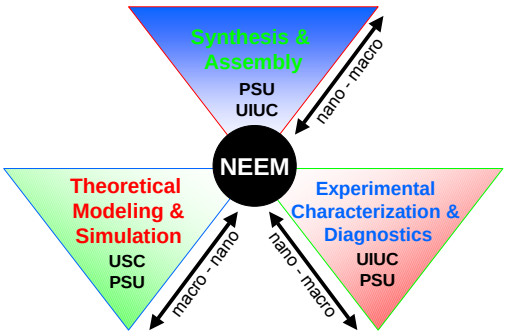

Figure 1. NEEM MURI program structure.

The second annual review meeting for the MURI program was held November 2006 in Aberdeen, MD. A summary of the meeting can be found at the MURI website (www.neem.psu.edu). The present report provides a brief description of scientific progress and accomplishments during the third year of the program. In addition, interactions and technology transfer among the team members and with DoD and DoE scientists are described. Finally, publications, presentations, and demographics of the program are reported.

Scientific Progress and Accomplishments

Synthesis and Assembly

The objective of this effort has been to develop new methodologies for synthesis and assembly of nano-structured energetic materials. The scientific challenges are twofold: Can self-assembly methods afford energetic nanoparticles that are stable against environmental degradation? Can one make energetic aluminum and boron nanoparticles by a bottom-up approach?

Boron Nanoparticles

Elemental boron is a highly attractive fuel for propellants and explosives. Of all the chemical elements, boron has the highest volumetric heat of combustion (33.4 kcal/cm^3) and the third highest gravimetric heat of combustion (14.1 kcal/g), after liquid H_2 and Be. These values are over 3 times higher on a volume basis and 1.4 times higher on a weight basis than those of hydrocarbon fuels. Boron is an extremely hard and refractory material (melting point of 2075 ºC; boiling point of 4000 ºC), which makes it imperative to render it into particulate form for use as an energetic material.

During the past year, **Nuzzo** and **Girolami** and their groups have developed the first convenient, clean, and simple preparation of boron nanoparticles by the gas phase pyrolysis of decaborane. Decaborane, $B_{10}H_{14}$, is an air stable crystalline solid that is known to decompose to give boron films on surfaces at temperatures as low as 200 ºC. Passage of decaborane vapor in an argon carrier at 1 atm through a hot zone at 700 - 900 ºC affords a grey-brown, non-pyrophoric powder. Microanalysis revealed that the powder consisted of 97.2 % boron, with traces (<0.5%) of carbon and no hydrogen. The particles are easily suspended in organic solvents such as toluene and settle slowly over a few hours.

TEM images show that most of the particles have diameters in the range 10 to 50 nm, with a few particles as large as 100 nm (**Fig. 2**). The particles lack texture and are approximately spherical shape. Diffuse rings (at d = 0.194±0.1 and 0.326±0.1 nm) are observed in the electron diffraction pattern (**Fig. 3**), and two broad peaks at 2θ = 22.5º and 35.0º were observed in the Cu Kα XRD pattern (**Fig. 4**). These peaks roughly correspond to the (111) and (121) Miller planes of β-rhomobohedral boron. A Scherrer analysis of the peak widths suggests that the crystalline domains are about 22 Å in size.

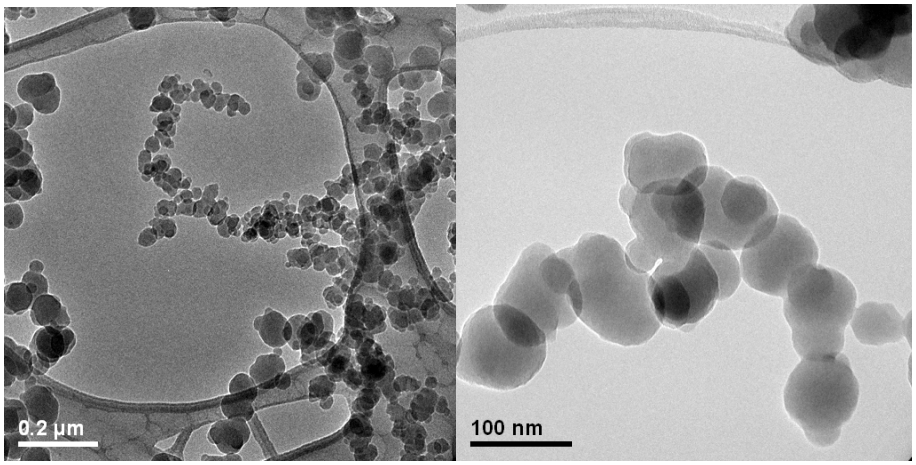

Figure 2. TEM images of the boron nanoparticles.

The energy content of the boron nanoparticles was determined by differential scanning calorimetry (DSC), in which the nanoparticles were heated in the presence of dry oxygen from 25 °C to 643 °C with a heating rate of 10 °C/ min. The DSC traces (**Fig. 5**) revealed a significant exotherm: the oxidation begins at 431 °C, peaks at 576 °C, and then rapidly stops. The total heat of oxidation is 17.2 kJ/g, which corresponds to about 30 % of the theoretical value, assuming that all boron atoms are converted to B_2O_3. Our data suggests, consistent with current literature understandings, that thermal oxide layers prevent the core boron atoms from oxidizing.

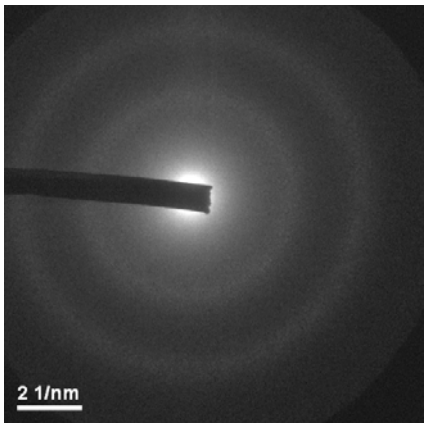

Figure 3. Electron diffraction pattern of the boron nanoparticles (200 keV).

The possibility of preparing surface-modified boron nanoparticles was examined. Treatment with bromine for 24 h and removal of the excess bromine at 50 °C under vacuum affords a dark grey powder with 4.0 - 9.6 % of bromine content. The Raman spectrum of the bromine-treated particles exhibits three bands at 212, 255, and 259 cm^{-1}. These bands disappear after washing with ether or after treatment with excess 1-octanol. Those bands in the Raman spectrum are due to the presence of Br_5^-, rather than bromide groups bound to the boron particles. No band at around 300 cm^{-1} due to bromine was evident. Current work is examining alternative approaches to functionalizing the surfaces of both these materials and compound phases that will be prepared using multicomponent precursor feeds (e.g., to incorporate Si) in the pyrolysis step. Our hypothesis is that these alloyed compositions will provide a means to manipulate the thermal oxidation processes as well as provide new chemistries for modifying the surfaces of the nanoscale materials prepared.

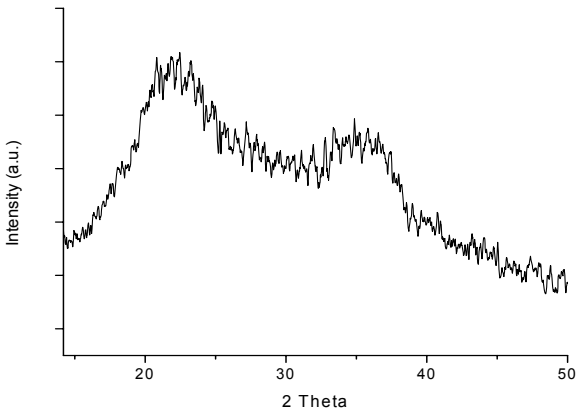

Figure 4. XRD profile (Cu Kα radiation) of the boron nanoparticles.

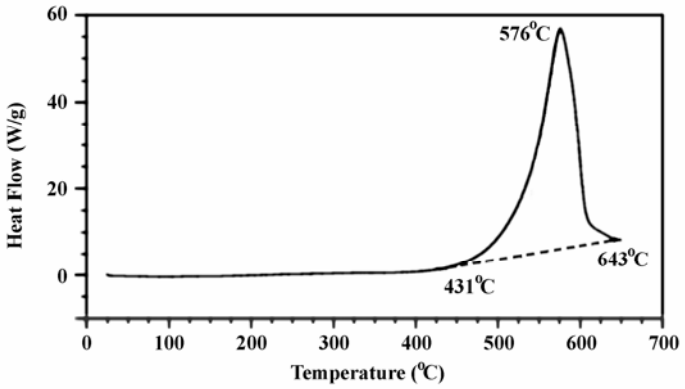

Figure 5. DSC traces of boron nanoparticles under oxygen atmosphere.

The key findings for this past year have been:

- The discovery of the first "bottom-up" method to make boron nanoparticles: gas phase pyrolysis of decaborane /Ar mix at 700-900 °C and 1 atm.
- The boron nanoparticles are pure (>97% B), easily suspended in organic solvents, and show diffraction peaks characteristic of β-rhombohedral boron with 20 nm crystalline domain size.

Chemistry and Structure of Al-SAM Surfaces

Allara and his group are using surface science and experimental chemistry methods to study the structures and energy releasing reaction pathways of nano-structured energetic materials (NEEMs). The specific objectives are (i) to develop new methods, using self-assembled monolayers (SAMs), to generate metal nanoclusters stabilized against environmental degradation while preserving high energy content, (ii) to structurally characterize specially synthesized nano-

energetic materials interfaces and assembled nano-structures, and (iii) to assist in combustion microanalysis of thermite and intermetallic nano-structured energetic materials.

The approach has been to synthesize oxidizer groups containing SAMs, especially those with NO_2 groups that are related to actual explosive materials such as TNT and RDX, and characterize the chemical and physical interactions with simple reducer atom beams or fluxes, especially Al atoms. State-of-the-art ultra high vacuum systems have been built for controlled flux atom depositions with temperature control of the samples. Diagnostic probes are being developed and applied for following the physical and chemical processes that evolve with creation of the oxidizer-reducer energetic interfaces and interphases.

During the last year, the **Allara** group rebuilt the Infrared Reflection Spectroscopy UHV chamber to a second (not final) stage design in an effort to better control the cooling of the substrate during Al atom (or other reducer atom) flux delivery. **Figure 6** shows the general outside view of the chamber and **Fig. 7** shows the interior of the metal deposition arm. Trial experiments were run that showed that ~120 K could be reached with this setup. Elimination of condensed background gases needs to be achieved by building an efficient cryo cooled sample shield. This setup was used in several experiments with dinitro aromatic SAMs and one aliphatic SAM, a simple model for explosives based on aliphatic structures such as RDX and HMX.

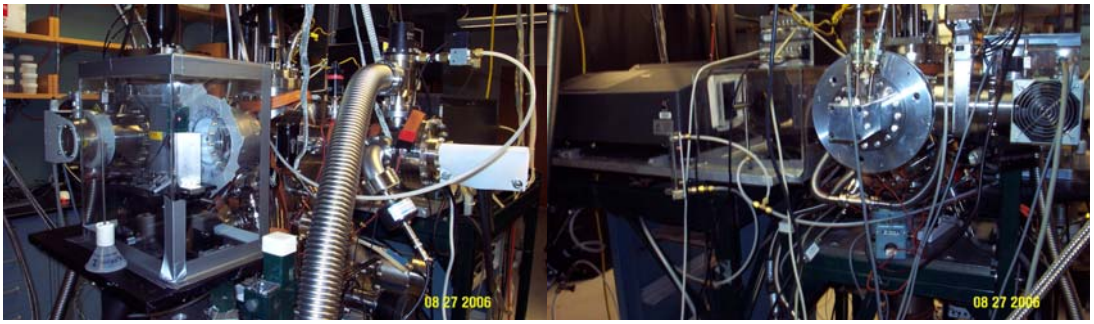

Figure 6. Detector optics (left) and infrared spectrometer (right) also showing the back of the metal evaporation system.

The general strategy and types of molecules being studied are shown in **Fig. 8**. The main dinitro compound studied, dinitrobenzoic acid, is also shown in the figure. During Al atom deposition, both nitro groups were reduced in parallel and temperature control down to ~150 K showed no evidence of changes in the reaction paths. Control experiments were run with K atoms, a 1-electron reducing agent which does not form covalent bonds, in contrast to Al atoms. The aliphatic molecule ω-nitropentadecanoic acid [$HO_2C(CH_2)_{13}CH_3$] was studied and the nitro group undergoes rapid reduction with Al atoms. XPS experiments need to be performed to determine the exact final chemical state of the interface product.

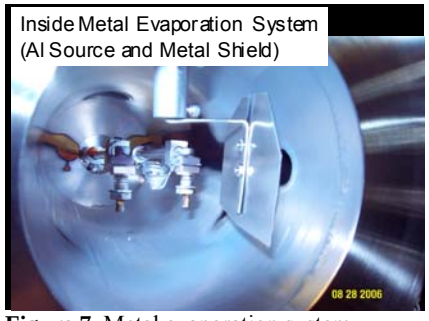

Figure 7. Metal evaporation system showing the Al source and metal shield.

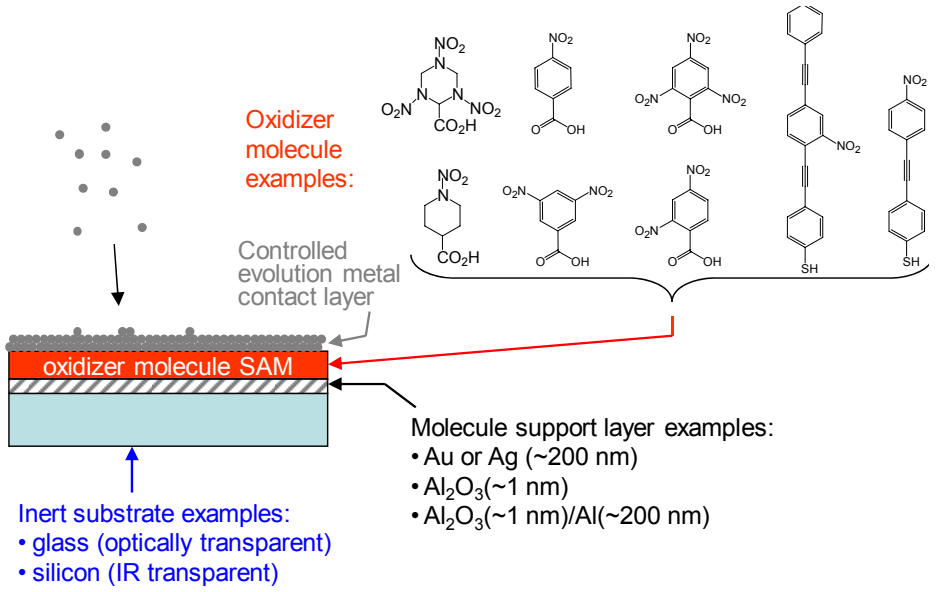

Figure 8. General strategy and types of molecules being studied

A method for formation of stabilized Al nanowires in a hydrocarbon SAM was also developed during the past year (**Fig. 9**). Deposition of Al atoms onto a dense, well organized alkanethiolate SAM on Au{111} [$H_3C(CH_2)_{15}S$-/Au] was carried out at room temperature in a UHV chamber interfaced to a high resolution atomic force microscope (AFM) probe capable of operating in contact, non-contact (NC), and conducting probe (CP) modes. By carefully controlling the number of Al atoms deposited per molecule a coverage of 3 Al atoms/molecule was determined at which most of the Al atoms were located at the Au-S interface and in the form of nanofilaments with diameters believed to be in the range of 1-3 aluminum atoms on average with lengths of ~2 nm. These wires, formed between the alkyl chains, were stable in vacuum for as much as 24 hrs with no reaction of the background O_2 gas (partial pressure ~10^{-8} torr). In comparison in the same vacuum chamber, freshly deposited Al on a bare surface starts forming oxide within minutes. This experiment indicates that Al atoms can be stabilized if buried within densely packed molecular films and presumably retain their high energy towards reaction with oxidizer molecules. The presence of the Al nanowires was determined by topography (contact and NC) modes with the best evidence from the CP mode in which the wires were shown to conduct electrically to the substrate ground plane, whereas isolated Al clusters on the surface were insulated from the ground plane. A schematic of the nanowires in the SAM is shown in **Fig. 9**. **Figure 10** shows a CP scan diagram and a resulting line scan of the current distribution across the

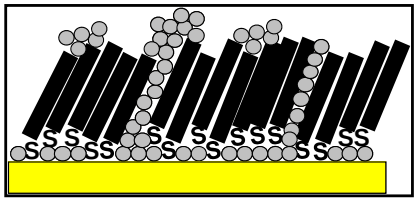

Figure 9. Illustration of stabilized nanowires in a hydrocarbon SAM.

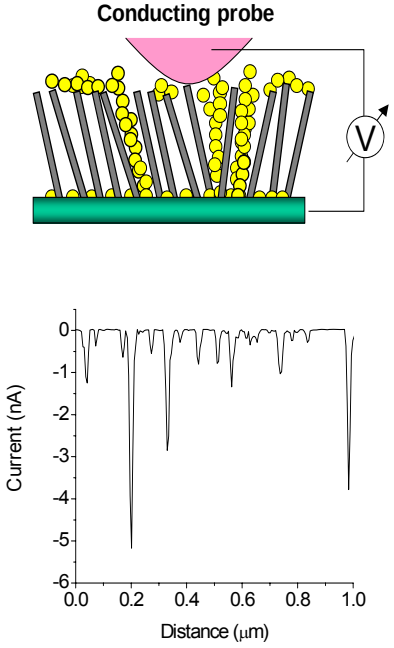

Figure 10. Conducting probe diagram (top) and line scan of filaments across surface (bottom).

surface. In the line scan, one can see the distribution of nanofilaments which conduct the current. Not all the nanofilaments have equal conductance which we ascribe to the varying diameter and to the extent of filament growth to the surface of the SAM (~2 nm thickness). Since the SAM has a density of chains near 4.6/nm^2, with a maximum separation between chains of ~0.05 nm when extended straight and vertical, and since no SAM molecules are lost in the process of Al deposition, this limits the sizes of the nanofilaments to almost no more than 1 atom in diameter. To be conservative, we limit the sizes to perhaps 2 Al atoms in diameter. These are the smallest form of Al atom clusters ever grown, to our knowledge, and offer an opportunity to study the reactivity of these high surface/volume forms of Al with respect to nanoenergetic materials.

Ultra-High Pressure Supercritical Fluid Processing of Nano-sized RDX

For all applications of energetic material, insensitivity to detonation is essential for safety. Armstrong et al. [1] suggest that a reduction in crystal size and elimination of crystalline imperfections can significantly reduce the sensitivity of the energetic material. Therefore, for supporting the future formulation of insensitive energetic materials, it is highly beneficial to synthesize nano-sized energetic particles with reduced imperfections.

Current techniques such as physical grinding are capable of reducing the crystal size down to the micron-scale and result in crystals with uneven particle size distributions, crystalline surface imperfections, and internal inclusions. Surface defects and sharp edges are clearly shown resulting from the shearing process. There is also the obvious safety concern due to the resultant frictional heating of the grinding process which may lead to explosion. Thus, it is desirable to utilize certain processing techniques, which are less intense in the heat generation and more controllable in terms of physical processes and particle recovery procedure.

This has led to the use of supercritical fluids (SCF) for the reduction of particle size. The RESS process has been shown to produce particles on the nano-scale [2,3]. Using the homogeneous nucleation theory of Debenedetti [4], it can be shown that as the degree of supersaturation increases, the critical nucleus size decreases. Therefore, as the critical nucleus size decreases more critical nuclei are formed, which results in small particles. The RESS process has been shown by Stepanov et al. [5] to be effective in the production of nano-sized RDX at relatively low pressures ($p \leq 29.5$ MPa).

To better understand the degree of supersaturation in the RESS process, the solubility of the solute in supercritical CO_2 needs to be known. While the solubility of many different solutes have been recorded in supercritical CO_2 in the past, the information on the solubility of many energetic materials including RDX is somewhat limited to narrow pressure and temperature ranges. Solubility measurements of RDX in dense CO_2 have been performed at pressures below 48.3 MPa by Morris [6]. To extend the pressure and temperature range beyond previously studied ranges, **Kuo** and his group designed and fabricated a solubility vessel so that the solubility of energetic materials in supercritical CO_2 could be characterized.

The overall objective of the effort by **Kuo's group** is to advance the state-of-the-art of the RESS process by achieving more in-depth understanding of the homogeneous nucleation process for nano-sized energetic particle synthesis. The specific objectives include: 1) development of suitable techniques for recovery of nano-sized energetic ingredients while avoiding agglomeration; 2) acquisition of solubility data of RDX for broad ranges of temperature, pressure, and solvent concentration; and 3) investigation of the dependency of recovered particle size on nozzle throat diameter and operating conditions.

An ultra-high-pressure RESS system was designed, fabricated, assembled, and tested. This system (**Fig. 11**) consists of several main components: 1) a 207 MPa high-pressure compressor, 2) a windowed high-pressure saturation vessel ($p \leq$ 207 MPa) with temperature control, 3) a heated expansion nozzle section containing an interchangeable nozzle elements with throat diameters varying from 100 – 340 μm, 4) a jet expansion tube for facilitating dry ice formation, 5) nano-sized particle collection vessel, 6) a scrubber for filtering RDX particles from exhaust gases, 7) a surge tank in an alternative exhaust line for discharging the high-pressure flow in the event of nozzle clogging, 8) a co-solvent feed system to the saturation vessel, and 9) a remotely operated control system with LabVIEW® control software and data acquisition unit.

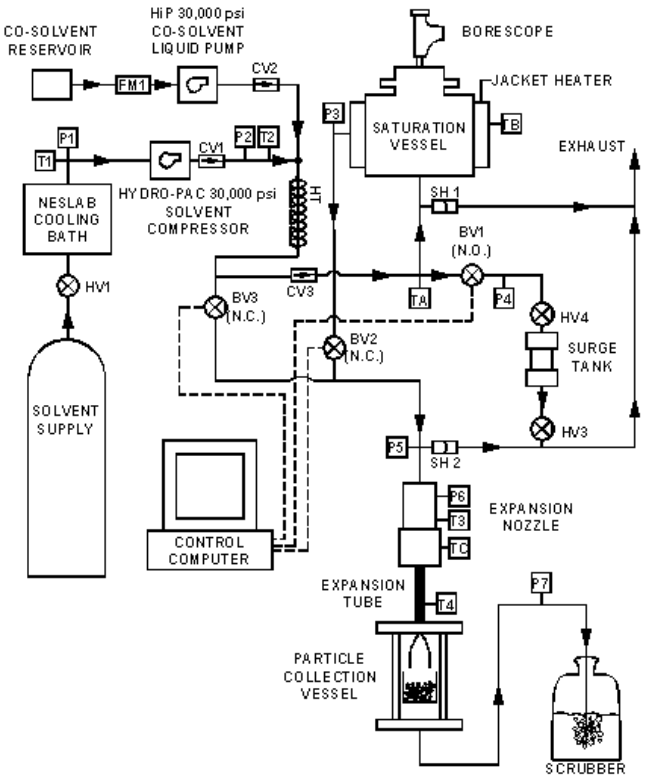

Figure 11. Process flow diagram of PSU's ultra-high-pressure.

In order to enhance the dissolution process, numerous 0.25″ glass beads were used to contain RDX as a coated layer on their surface. This procedure greatly increased the surface area over which the CO_2 and the RDX could interact. A transparent particle collection vessel was designed to connect to the downstream end of the expansion tube, which facilitates the formation of dry ice during the homogeneous nucleation process. The collection vessel consisted of a removable particle container, a clear acrylic outer wall for viewing the motion of the dry ice exiting the expansion tube, and a supporting stand for the particle container in order to allow any remaining CO_2 gas to escape from the particle collection vessel. The exhaust gas was then guided through a water bath in the scrubber for removing any RDX particles entrained in the exhaust gas. After the RESS process, the particle collection container was removed prior to the sublimation of accumulated dry ice. In this manner, high percentages of nano-sized RDX are still contained in the dry ice. The dry ice is allowed to sublimate leaving the RDX particles behind in the collection container. Samples were then properly stored for analysis.

The free jet created through the converging nozzle produced a rapid expansion of the supercritical solution and resulted in homogenous nucleation of the RDX particles from the solution. To understand the conditions at specific points in the flow, an in-depth flow analysis was necessary. By simply approximating the expansion jet as an ideal gas without solute, an estimate of the jet geometry and properties was obtained through a CFD simulation using the Fluent® Code (**Fig. 12**). The ideal gas assumption is partially justifiable due to the low concentration of the RDX solute in the expansion jet.

One of the major challenges encountered in the RESS process was the collection of generated nano-sized RDX particles. These ultra-fine particles can easily be entrained by the flowing CO_2 discharging from the system. Also, nano-sized particles tend to coat the walls of the

expansion tube and the collection vessel. The handling of ultra-fine RDX particles must avoid generation of sparks due to any static charges. Friction can also cause the final products of the RESS system to reach ignition conditions. Special care must be taken when handling all recovered materials. One consideration was the use of filtration in the exhaust lines to extract the RDX particles from CO_2 gas entrainment. However, not only is the active filtration of nano-particles difficult but the resulting flow restriction greatly inhibited the velocity of the exhaust gas.

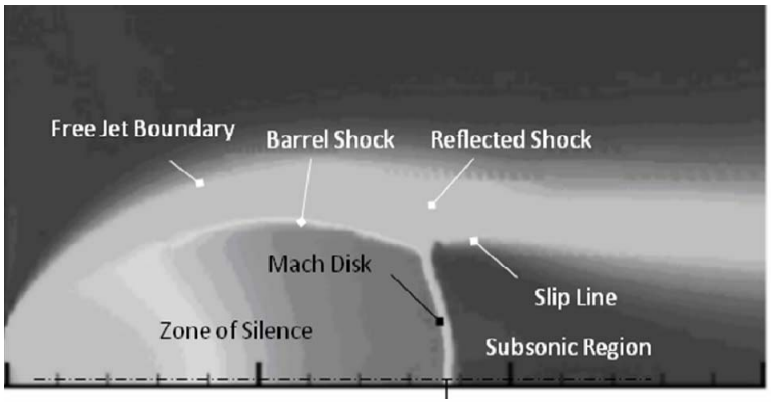

Figure 12. Calculated free jet expansion of CO_2 treated as an ideal gas without solute.

After various iterations, the method adopted in collecting ultra-fine particles was the formation of dry ice (solid CO_2) in the expansion tube downstream of the nozzle exit and in the particle collection vessel. Eventually, CO_2 enters into the solid phase when its temperature is below its freezing point. The driving force for homogeneous nucleation of RDX particles exists along the rapid expansion path. Due to the heterogeneous nucleation of dry ice with RDX particles serving as nuclei, RDX particles are encapsulated in dry ice. This process prevents RDX particles from coagulating early in the particle growth process. With the use of a constant-area tube for confining the expanding jet, the CO_2 flow was forced to reach high concentrations and greater probability for the formation of CO_2 critical nuclei, which facilitate the formation of dry ice. Due to coagulation of CO_2 particles, larger chunks of dry ice can form. These large chunks are affected by gravity with less chance for entrainment by the exhaust gas. The end result of the rapid expansion and growth processes leads to larger dry ice particles, which contain numerous nano-sized RDX particles. Thus, the formation of dry ice is beneficial for collection of nano-sized RDX particles.

A high-pressure solubility measurement system with temperature control and a magnetic stirring agitator was designed, fabricated, and tested to measure the solubility of energetic materials in supercritical CO_2 (**Figs. 13** and **14**). The main chamber is composed of a cylindrical nitronic-50 vessel with a brass sliding piston which is driven by hydraulic oil on one side to change the volume of the solubility measurement compartment. The hydraulic oil line is connected to a hand pump that is safely located outside of the test room. A tape heater is used to control the temperature of the solution. The magnetic stirrer is utilized to ensure the solution is well mixed and is at a uniform temperature. The temperature and pressure inside the solubility measurement compartment are monitored with a thermocouple and a pressure gauge. A sapphire window is housed in the end-closure component of the compartment to enable visual observation of the

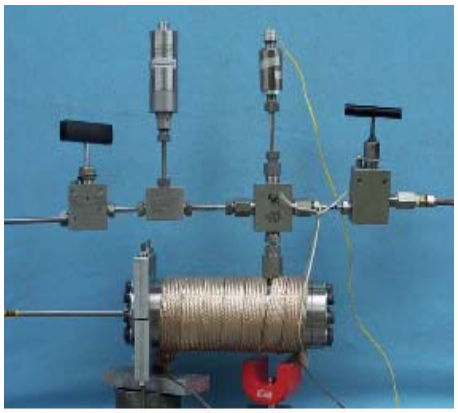

Figure 13. Photograph of solubility measurement vessel and adjacent components.

solution through a borescope, which is linked to video camera for recording purpose. Prior to the start of the solubility measurement tests, a known amount of RDX particles is loaded into the compartment, then liquid CO_2 is fed into the vessel by the opening of hand valves HV1 and HV2. After closing all inlet and exit hand valves, the pressure in the solubility vessel is then gradually increased by the manually pumping of the hydraulic oil to drive the sliding piston into the compartment containing CO_2 and RDX solution. Once the pre-specified operating condition is attained and all RDX is dissolved in the supercritical CO_2, then by gradually releasing the hydraulic oil pressure using the manual valve MV1, the piston slides away from the compartment, decreasing the pressure in the CO_2/RDX solution, while holding the temperature constant. When the solution reaches the threshold pressure for total RDX solubility at this pre-specified temperature, a cloud point suddenly appears. This cloud point indicates the solubility limits of pressure and temperature for the initial concentration of RDX. This process is then repeated for higher temperatures to obtain additional solubility data with the same initial concentration. After the test has been completed, the solution can be discharged through exhaust line to the scrubber when the hand valve HV3 is opened.

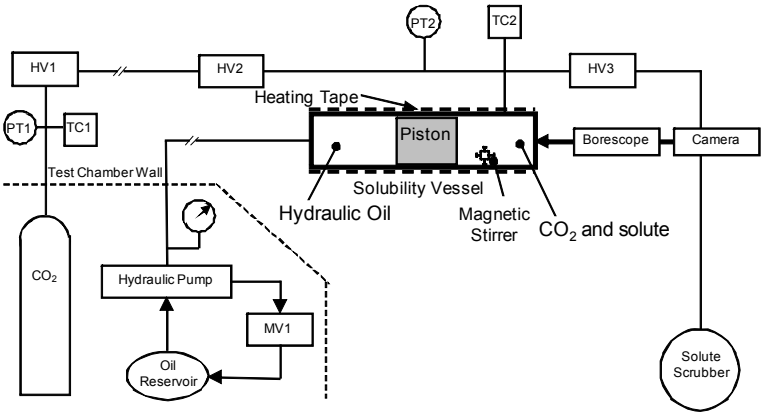

Figure 14. Schematic diagram of the solubility measurement system.

The majority of the RESS tests were performed using a 316 stainless steel converging nozzle with an exit diameter of 340 μm. Due to the relatively large diameter of the nozzle throat, the high-pressure compressor was unable to supply sufficient CO_2 mass flow rate at an elevated pressure. However, when the 100 μm diameter nozzle was used, a steady high-pressure condition at upstream potion of the nozzle was achieved. Tests reported here were performed at a nominal pressure of 34.5 MPa with saturation vessel temperatures ranging from 65°C to 80°C. Test conditions are summarized in **Table 1**.

Table 1: Test summary of RESS process for ultra-fine RDX particle synthesis

Test	Sample Size [mg]	Nozzle Throat Diameter [μm]	Pressure [MPa]	Temperature [°C]	Mean RDX Diameter # [nm]
RDX-001	52	340	33.1	66	509
RDX-002	70	340	33.8	79	93
RDX-003	55	100	36.9	65	248
RDX-004*	80	100	N/A	N/A	N/A
RDX-005	79	340	26.0	81	265
RDX-006	58	340	27.1	75	195
RDX-007	51	200	103.4	95	126

* Note that RDX-004 was unable to be completed due to nozzle clogging.

Note that the measured size by the Nanosizer may be affected by the effect of particle agglomeration, especially for RDX-001.

To analyze the recovered samples, a Malvern Nanosizer was used in the determination of the particle size distribution. RDX samples were first suspended in de-ionized water. The sample was then sonicated in an ultrasonic bath in order to break large agglomerates and evenly disperse RDX within the water. A small amount of the mixture was then placed into the Nanosizer. Particles move and diffused as a result of solvent motion. Particle diffusion was then measured by a non-invasive technique called Dynamic Light Scattering (DLS) technique.

The DLS technique measured the intensity of the scattered light and resolved the diffusion coefficient and particle size using an intensity correlation function. All samples were analyzed multiple times and mean values of diameter were established. The results are also tabulated in **Table 1**.

A JEOL 6700F type FE-SEM was used in order to obtain images of all the samples collected. The SEM image shown in **Fig. 15a** shows the morphology of preprocessed military grade RDX crystals at a 3.2k magnification before they are put through the RESS process. The SEM image shown in **Fig. 15b**, indicated non-uniform RDX particles synthesized using a 340 μm nozzle throat diameter in the RESS process under test conditions specified by RDX-001; the

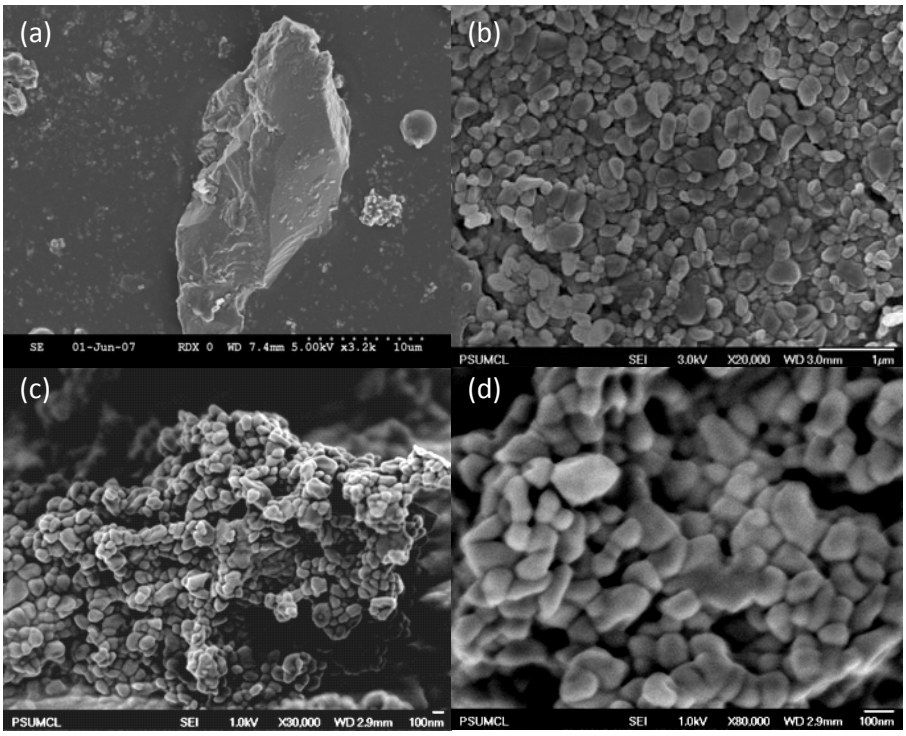

Figure 15. SEM images of RDX particles. (a) recrystallized military grade RDX sample at 3.2k magnification, (b) synthesized RDX particles from Test RDX-001 at 20k magnification, (c) synthesized nano RDX particles from Test RDX-007 at 30k magnification, and (d) synthesized RDX nano particles from Test RDX-007 at 80k magnification.

particle sizes ranged from 85 to 504 nm. RDX-001 was conducted at approximately 33 MPa and the saturation vessel contained 50 mg of RDX. Another SEM image, shown in **Fig. 15c**, also indicates relatively uniform particle size synthesized in the RESS process under test conditions specified by RDX-007; the particle sizes ranged from 104-147 nm. RDX-007 also used 50 mg of RDX, however, the saturation vessel pressure was approximately 103 MPa and the temperature was approximately 95°C. The nozzle throat diameter was 200 μm for test RDX-007. For this test, the container (with the recovered RDX particles and dry ice) was put in a vacuum desiccator

to try and reduce the amount of moisture absorption by the RDX particles. A high-magnification image of particles from test RDX-007 is shown in **Fig. 15d**.

To summarize the effort on supercritical fluid processing of nano energetic crystalline oxidizers by the **Kuo group**, an ultra-high-pressure RESS system with controlled temperature and pressure was developed and tested to produce nano-sized RDX particles. Demonstration test runs showed that even using a relatively large nozzle with a throat diameter of 340 μm, the system was capable of generating nano-scale particles at high pressures (~34.5 MPa) and moderately elevated temperatures (65°C to 80°C). At the present time the number of tests is relatively low, since the ultra-high-pressure RESS system was established very recently. Even though a full picture of the effect of temperature, pressure, and nozzle throat size on the synthesized RDX cannot be established, some trends can be seen by comparing the current test results. For example, in comparing tests RDX-001 and RDX-003 for which the nozzle throat is smaller in the latter, a reduction in the particle size is observed. It is advantageous to use smaller diameter nozzles in producing nano-sized particles while maintaining a constant upstream pressure before the exit nozzle. Another observation is that for a given sample size, higher temperature in upstream region of the nozzle seems to have a stronger effect on RDX particle size (see RDX-001 and RDX-006 in Table 1). This can be explained by the stronger dependency of solubility on temperature than pressure. It is believed that the attainment of a higher degree of supersaturation is of the greatest importance in producing nano-sized RDX particles. Up to now, the different nano-sized RDX particles ranging from 93 to 509 nm were obtained from the demonstration runs under various controlled conditions, using different nozzle sizes, upstream temperatures and pressures.

This ultra-high-pressure RESS system has been shown to have high percentage of particle recovery, typically ~90% of material placed initially in the saturation vessel. Efficient particle collection was also achieved through the use of an expansion tube facilitating the formation of dry ice. Any RDX materials not dissolved in the supercritical CO_2 were found to be retained on the glass beads in the saturation vessel. The use of dry ice has also proven to be a safe way of handling the recovered samples as the RDX particles are retained in a very low temperature environment. The use of high-pressure operating conditions appears to have a positive effect on the enhancement of solubility of RDX in dense CO_2 but further study is needed to quantify the degree of benefit.

Electrostatic Self-Assembly of a Nanoscale Thermite System into ordered Microspheres

The **Yetter group** in collaboration with **Dr. Tim Foley** of Los Alamos National Laboratory has used electrostatic self-assembly to create a nanoscale thermite system from nAl and nCuO particles. The nAl had a spherical shape with a nominal particle diameter of 38 nm and an active aluminum content of 49%. The nCuO particles were spherical with a nominal particle size of 33 nm. Ligands with a positive or negative ω-functionalization were attached to the surface of each nanoparticle to create a charged self-assembled monolayer (SAM). The ligand used to functionalize the surfaces of the aluminum particles was an ω-trimethylammonium (TMA) functionalized carboxylic acid, $HOOC(CH_2)_{10}NMe_3^+Cl^-$. The nCuO surfaces were treated with the ω-carboxylic acid functionalized thiol, or mercaptoundecanoic acid (MUA), $HS(CH_2)_{10}COOH$. The positively charged nanoaluminum and negatively charged nanocupric-oxide were each suspended in a separate solution and upon mixing the two constituents, they self-assembled into microspheres with diameters on the order of 1 μm. Examples of the micron-sized composite particles formed are shown in **Fig. 16**. These self-assembled nanothermite microspheres (SANTMs) are the first known energetic thermite systems created from the bottom-

up. This method allows for the mixing of the two constituents to be performed without sonication, and could potentially create a highly ordered system with minimal diffusion distances between the two constituents. These self-assembled nano thermite micro spheres (SANTMs) are essentially an ordered matrix of nAl and nCuO particles held together by an infrastructure of long carbon chains. This is ideally how a heterogeneous energetic material with a carbonaceous binder should be created to ensure maximum performance. Gaining a better understanding of this type of nanoscale manipulation and construction will allow for specific tailoring of the burning characteristics by varying the most fundamental of building blocks.

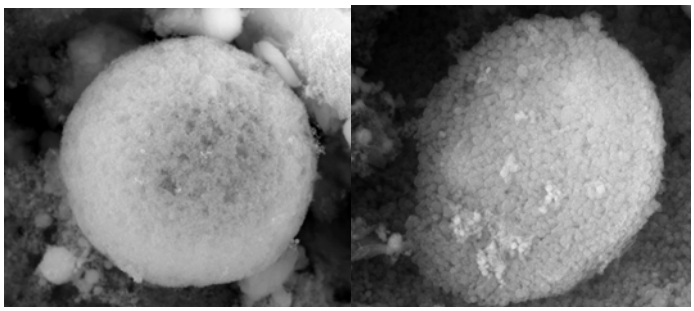

Figure 16. SEMs of nAl and nCuO self-assembled nanothermite microspheres (SANTMs). The particles shown are a few micron in diameter.

Theoretical Modeling and Simulation

A goal of this portion of the MURI project is to study nano-engineered energetic materials using large (*billion atoms*) multiscale simulations that couple quantum-mechanical (QM) calculations to molecular dynamics (MD) calculations. The **USC group** (**Vashishta, Kalia,** and **Nakano**) is calculating the stability, structure and energetics of metallic nanoparticles with a special focus on the relationships between particle size, shape and excess surface free energy. Multiscale modeling of the thermo-mechanical properties and microscopic mechanisms of detonation and deflagration processes of NEEMs is also being studied. These calculations couple directly to the synthesis, fabrication, and materials characterization studies of **Allara, Nuzzo,** and **Girolami** as well as to the dynamical characterization studies of **Dlott** and **Yetter.** Theoretical studies by **Yang** will couple to the studies of the **USC group** at the meso/macro scale. **Yang** is also modeling the supercritical fluid processing techniques understudy by **Kuo and colleagues**.

During the past year, the **USC group** has continued to advance their scalable reactive molecular-dynamics methods to study the shock compression of self-assembled monolayers and the flash heating of an alumina nanoparticle.

Scalable Reactive Molecular-Dynamics Methods on World's Fastest Supercomputers

High-end computing platforms such as the 131,072-processor IBM BlueGene/L at the Lawrence Livermore National Laboratory and the 10,240-processor SGI Altix 3000 at the NASA Ames Research Center provide an excellent test grounds for the **USC group's** linear-scale algorithms for multimillion-atom MD simulations to study the interplay between chemical reactions, long-range stress fields, and microstructures such as voids and grain boundaries. On these platforms, unprecedented scales of quantum-mechanically accurate and well validated, chemically reactive, atomistic simulations have been achieved—1.06 billion-atom fast reactive force-field MD and 11.8 million-atom (1.04 trillion electronic degrees-of-freedom) quantum-mechanical MD in the framework of the embedded divide-and-conquer density functional theory on adaptive multigrids—in addition to 134 billion-atom non-reactive space-time multi-resolution MD, with the parallel efficiency as high as 0.998 on 131,072 BlueGene/L processors (**Fig. 17**).

Shock Compression of Self-Assembled Monolayers

The molecular mechanics behind high strain-rate deformations of self-assembled monolayers (SAMs) has a number of practical applications such as high explosives near detonation front. Recent advancements in shock spectroscopy and large–scale atomistic simulation techniques have enabled direct comparison of experimental and simulation result on the relevant time and length scales. In pioneering experimental work in **Dlott's group** at the University of Illinois, ultrafast shock wave compression experiments of alkanethiol SAMs with sum frequency generation (SFG) spectroscopy probed instantaneous orientations of the terminal methyl groups. It was observed that the SAMs with an even number of methyl groups (n = 14 in -S-$(CH_2)_n$-CH_3) completely recover the SFG signal intensity after the shock passes through, while the SAMs with an odd number of methyl groups (n = 17) only partially recover the initial SFG signal intensity.

The **USC group** has performed large-scale parallel molecular-dynamics (MD) simulations with an all-atom model to study shock compression of alkanethiol SAMs on Au (-S-$(CH_2)_n$-CH_3 with n = 11—17); see **Fig. 18.** Shock-induced structural changes have been investigated as a function of temperature T and molecular chain length n. For SAMs without any external compression, simulation results reveal an "even-odd" effect at low temperatures. Even-n SAMs have larger methyl tilt angles and larger gauche defect density than the odd-n SAMs (**Fig. 19**). Under shock compression the methyl tilt angles for even-n SAMs are larger than for odd-n and the "even-odd" effect for the methyl tilt angles remains unchanged. While shock compression induces gauche defects in the molecular chains of all lengths, even-n SAMs have lower defect density than odd-n SAMs therefore inverting the "even-odd" effect for gauche defects into the "odd-even" effect under shock compression (**Fig. 20).** The **USC group's** MD simulations thus

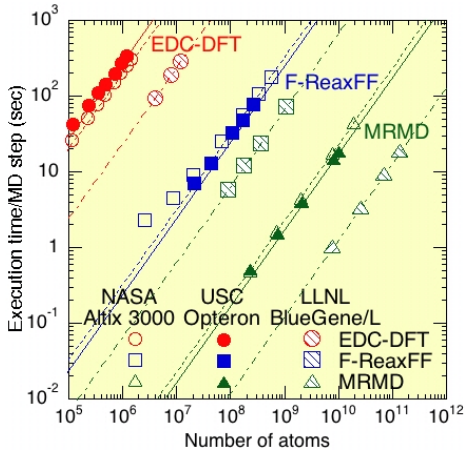

Figure 17. Benchmark tests of USC's reactive and nonreactive MD simulations on 1,920 Itanium2 processors of the Altix 3000 at NASA (open symbols), 2,000 Opteron processors at USC (solid symbols), and 131,072 BlueGene/L processors at LLNL (shaded symbols). The execution time per MD step is shown as a function of the number of atoms for: quantum-mechanical MD based on the embedded divide-and-conquer density functional theory (EDC-DFT, circles); fast reactive force-field MD (F-ReaxFF, squares); and nonreactive space-time multiresolution MD (MRMD, triangles). Lines show $O(N)$ scaling.

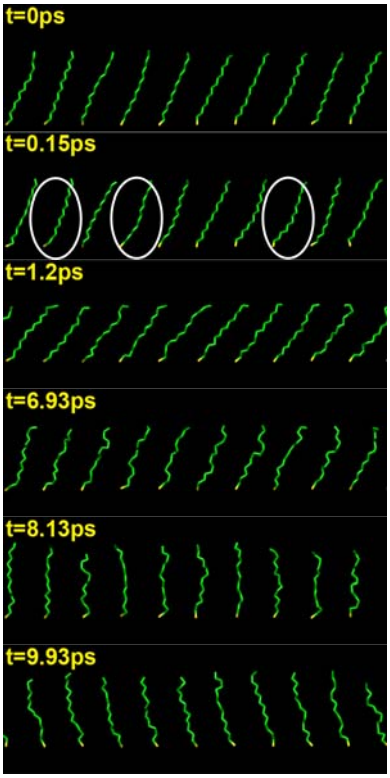

Figure 18. Snapshots of partial SAMs system for n = 13 at t = 0, 0.15, 1.2, 6.9, 8.13 and 9.93 ps during the shock simulation at 300K. C-C bonds are in green, S-C bonds are in yellow. Circled chains in the snapshot at t = 0.15 ps are typically curled when shock enters the system.

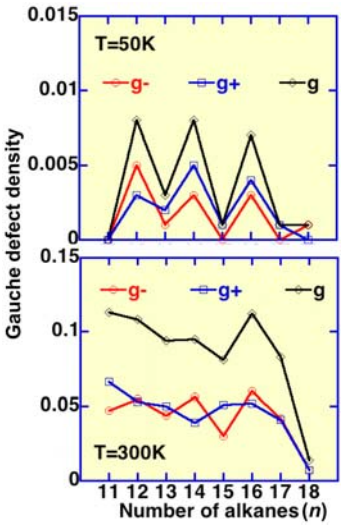

Figure 19. "Even-odd" effect in gauche defect density in uncompressed SAM chains (n = 11 to 18) at T = 50K and 300K. Black line with diamonds is the total gauche defect density (sum of g+ and g-), red line with circles is g-, and blue line with squares is g+.

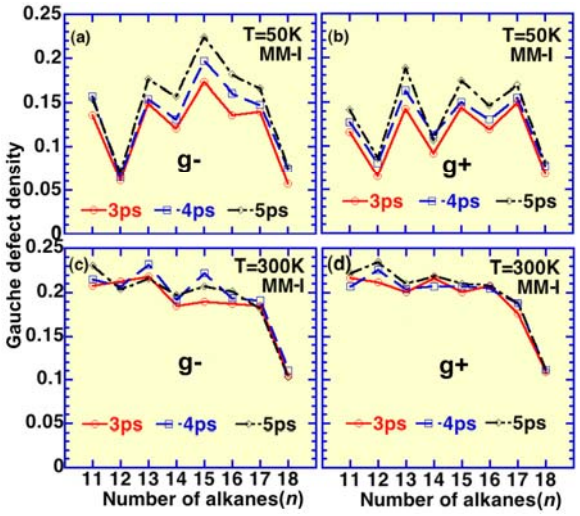

Figure 20. Shock-induced ""odd-even" effect in gauche defect density (g-: (a) and (c); g+: (b) and (d)) as a function of the number of alkanes at T = 50K ((a) and (b)) and 300K ((c) and (d)). Each plot contains data at three times: 3ps (circle), 4ps (square), and 5ps (diamond).

reveal a shock-induced inversion of the even-odd effect in the gauche-defect density. Temperature has a strong influence on this effect: the difference of methyl tilt angles, as well as the number of shock-generated gauche defects, between even-n and odd-n SAMs becomes less pronounced at higher temperatures.

Flash Heating of an Alumina Nanoparticle

Due to the enormous energy release associated with the formation of a more stable oxide by the reduction/oxidation (redox) reaction, reactions between a metal and an oxide have promising energetic material applications. To achieve high reaction rates through increased contact areas between fuel metals and reactant oxides, nanostructured composite materials have been developed. Recent experimental studies on the combustion properties of nanocomposites, such as Al+Fe_2O_3 and Al+MoO_3, have shown that flame propagation speeds reach km/s when the size of Al nanoparticles is reduced to less than 100 nm, in contrast to cm/s for traditional composites. The fast reaction of the nanocomposites cannot be explained by a conventional mechanism based on the diffusion of Al and O atoms in oxides. Instead it has been suggested that the fast flame propagation is due to spallation of the oxide shell covering the melted Al nanoparticles.

To study the mechanical response of an oxide shell to a high pressure generated by melting of an Al core, the **USC group** has performed large-scale chemically reactive MD simulations to study flash heating of a spherical aluminum particle of diameter 40 nm coated with an aluminum oxide shell of thickness 4 nm. In the flash heating simulation, the Al core is heated up to 3,000 K. The simulation shows the melting and evaporation of Al, followed by the rapid expansion of the oxide shell and its eventual failure (**Fig. 21**).

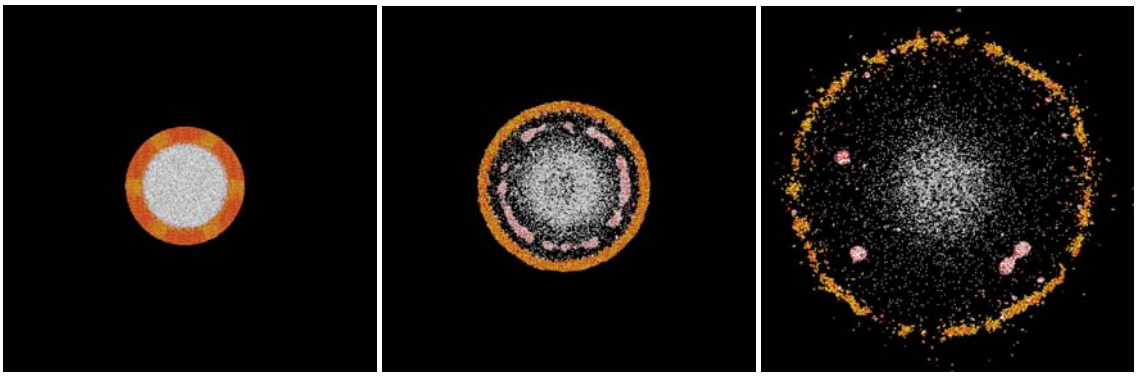

Figure 21. MD simulation to study flash heating of an oxidized Al nanoparticle. Snapshots at time 0 ps (left), 40 ps (middle) and 70 ps (right), where white, yellow and red spheres are Al atoms in the metal Al core, Al atoms in the oxide shell and O atoms, respectively.

Such an atomistic description of the initial reactions in nanoenergetic materials is vital for understanding the fast reactions found in nanothermite composites, which should be amenable to experimental measurements based on laser flash heating and picosecond spectroscopy by the **Dlott group** at the University of Illinois.

In summary, the large-scale MD simulations of the **USC group** have revealed: 1) shock-induced inversion of even-odd effect in the gauche-defect density in self-assembled monolayers; and 2) atomistic processes of flash heating of an oxidized Al nanoparticle.

The understanding gained in these simulations concerning material and mechanical behavior at the nanoscale will lead to the development of new and improved materials and structures with enhanced energy density and reduced sensitivity for a wide range of DoD applications. With the availability of tera-to-petaflops parallel platforms integrated with real-time 3D visualization and data analysis, it is feasible to carry out *Grand Challenge* simulations of materials properties and processes that can significantly accelerate the pace of experimental research in designing novel nanomaterials for defense applications.

Aluminum Nanoparticle Melting

Before moving to a full multi-scale modeling with simulations of the generation, transport, and combustion of nano-sized energetic materials, basic understanding of the combustion of a single particle in a quiescent medium is required. Many fundamental issues concerning the ignition and combustion characteristics of aluminum at nano-scales remain to be clarified. Moreover, the theories developed for micron-sized particles cannot be directly applied to study the ignition and combustion of nano-sized particles. There is a diversity of opinions regarding the ignition of these particles at small scales. The overall aim of the effort by the **Yang group** is to establish a unified theory accommodating the various processes and mechanisms observed at micro and nano-scales. Such a theory not only helps understand the behavior of a single particle, and can also act as a sub-model in predicting the collective behavior of particles at large scales.

A prerequisite to future development of nano-structured energetic materials is thorough understanding of structures that provide desirable performance, thermo-mechanical, and ignition and combustion characteristics. In light of the inconsistency and uncertainties of existing theories concerning the particle behavior at nano scales, fundamental research based on well-calibrated techniques appeared to be imperative. As a first step, the themo-mechanical characteristics such

as melting of particles over a broad range of scales need to be investigated. The melting of aluminum core and oxide layer plays an important role in determining the ignition characteristics of the particle. From materials perspective, melting is also one of the most important thermodynamic properties to characterize the material behavior. Although the thermodynamic aspect of melting is well recognized, the detailed mechanisms of melting are difficult to be established microscopically through experiments and still not completely understood. Due to the lack of experimental evidence in support of these models, there is speculation about the initiation mechanism of melting. Molecular dynamics studies, however, are free from such limitations and can provide detailed information about the time evolution of the system at the atomistic level, providing unique insight into the phenomenon. Since the presence of surfaces play a crucial role and act as a nucleation site for melting, a quantitative knowledge base and an alteration in the surface properties can have a major impact on the melting and related phenomena for the substance.

A comprehensive review on aluminum particles at micro and nano-scales was performed by **Yang** and his group during the first year of this project. Different processes involved during the ignition and combustion of these particles were identified. Research focus in the second year was placed on the continued development of a unified theory of particle ignition and combustion, and on the establishment of a Molecular Dynamics (MD) computational framework to handle processes and mechanisms at nano-scales. With the theoretical and computational tools already established, the main objective of this year was to investigate the thermo-mechanical behaviors of bulk and nano-particulate aluminum systematically by means of MD simulations. An optimum potential was selected to accurately and efficiently predict the melting of nano-scale aluminum particles. The effect of particle size was explored in the range of 2-9 nm.

The thermo-mechanical behavior of bulk and nano-particulate aluminum was investigated systematically by means of isobaric-isoenthalpic (NPH) simulations using the general computational framework developed in the previous years. The effect of voids and surfaces on the melting of bulk and nano-particulate aluminum was studied using MD simulations. For bulk materials, crystals composed of 864 and 2048 atoms were considered, and for particulates, spherical nano particles up to 8.5 nm (20736 atoms) were treated. The phenomenon of defect nucleated melting was studied using voids of different shapes and sizes and results were compared with pure crystals with no voids. The mechanisms of melting were examined using snapshots of the time evolution of atomic positions and density contours. The simulations were carried out by arranging atoms in an FCC lattice structure and evolving the system with periodic boundary conditions. The term melting point has been used in the literature with different definitions. Experimental melting point is the temperature for phase transition as observed in an experimental set up. Thermodynamic melting, T_m is based on the coexistence of the solid and liquid phase. In most of nucleation studies, the absence of nucleation sites in a perfect crystal leads to heating the substance beyond T_m, a phenomenon known as superheating. Structural melting refers to the limit beyond which there is a general collapse of lattice structure.

To study the effect of defects, crystals with different void sizes in the range of 0.19-4.0 nm^3 were considered in a bulk with 864 atoms. The influences of void shape and location were also treated. Voids provide a nucleation site for simulating the thermodynamic melting. However there is a range of critical void size for thermodynamic melting. A very small void size is insufficient for nucleation of the liquid phase, and a void size larger than the critical value can cause a collapse of the crystal. As compared to 1244 K for a pure crystal, the melting point for a crystal with voids initially decreases with void size, but eventually attains a plateau region at 960 K as seen in **Fig. 22**. This is very close to the thermodynamic melting of aluminum, i.e., 940 K in case of 864 atoms. The observation of a plateau region is consistent with those in the previous

studies on argon and copper. The critical void size of 1-1.7 nm^3 is sufficient enough to avoid superheating of crystals by providing a nucleation site for the liquid phase beyond which there is sudden collapse of the crystal. The melting temperature is only a function of the volume of the void but not its shape.

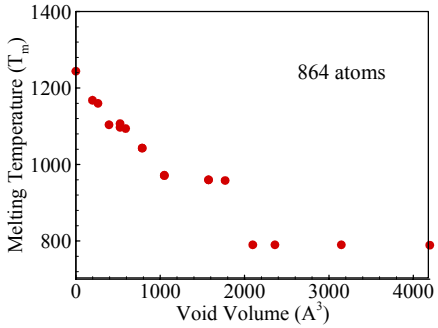

Figure 22. Effect of void size on melting of bulk aluminum consisting of 864 atoms using periodic boundary conditions.

The effect of the number of atoms in bulk on defect nucleated melting was studied by considering a bulk crystal with 2048 atoms. It was observed that the structural and thermodynamic melting points (plateau region) are identical to those for 864 atoms. The structural melting point for a pure crystal is observed at 1244 K, and the melting point decreases as the void size increases. The ratio between the structural and thermodynamic melting points ($f = T_s/T_m$) for aluminum is 1.32, close to 1.234 for such metal as copper. Moreover, the range of the critical void size increases as the number atoms considered to represent the bulk phase increases. For 2048 atoms, the void size of the order of 2-5 nm^3 results in thermodynamic melting, as compared to 1-1.7 nm^3 for 864 atoms. The aforementioned analyses were done in vacuum. The effect of pressure was also investigated by conducting the simulations at 1, 5, 10, 50, 100 and 300 atm. The pressure was found to be negligible and the same melting temperature was observed for all the cases.

Figure 23 shows the temporal evolution of atomic positions. The collapse of the crystal illustrates the difference between the structural and thermodynamic melting. In the former case, the phase transition is abrupt and homogeneous. As seen in **Fig. 23(a)**, the crystal has a solid structure till 124.2 ps, and a phase change occurs suddenly at 126.9 ps due to vibrational instability. However, in case of thermodynamic melting, nucleation starts near the void, as can be seen from the local concentration of atoms around the void, and proceeds to the rest of the crystal. **Figure 23 (b)** shows thermodynamic melting with a void of size 1.05 nm^3. The nucleation starts at the void at 85.8 ps and by 102.3 ps the whole crystal melts. If the void size is increased even further beyond its critical value, the whole crystal collapses and cannot be put in the category of either thermodynamic or structural melting. The breakdown of the structure can be seen in **Fig. 23 (c)** and is comparatively different from the mechanism of structural or thermodynamic melting. At 78.9 ps, when the temperature of the crystal is around 790 K, the atoms next to the void (4 nm^3) leave their positions and fill up the void space. No phase change is observed in this case.

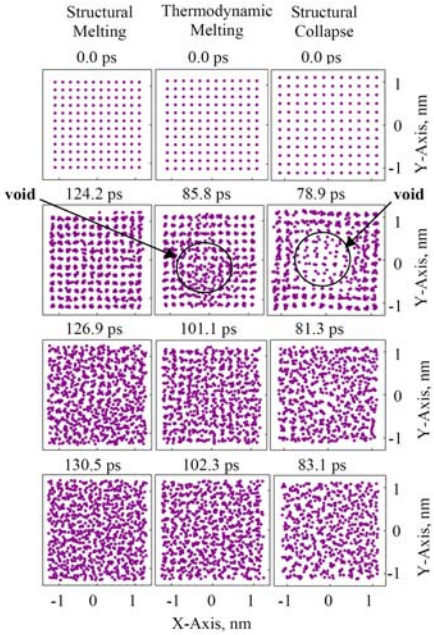

Figure 23. Temporal evolution of atomic positions showing mechanism of melting.

Particulate aluminum with diameters up to 8.5 nm was considered. No structural melting was observed because of the presence of surface acting as a nucleation site for the liquid phase. The effect of voids is also explored with sizes up to 14.1 nm^3. **Figure 24** shows the effect of void size on the melting of a spherical particle of size 8.5 nm. The melting temperature remains

constant till the void volume exceeds 5 nm^3 and then starts dropping as the void volume increases. Since surfaces are already present for nucleation, the presence of extra void just acts as another nucleation site and the phase change still occurs at thermodynamic melting point. As the void size increases, however, the particle is unable to contain the unstable forces due to the void and the phase transition occurs at a very low temperature of as low as 700 K for 10 nm^3 void.

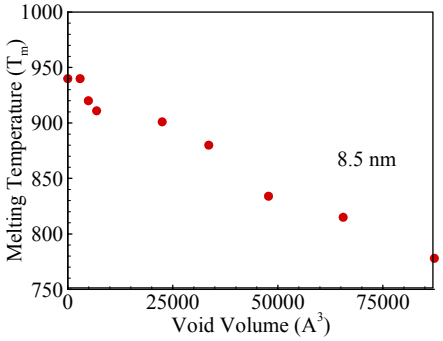

Figure 24. Effect of void size on melting of 8.5 nm aluminum nano particle.

The melting phenomenon can also be seen through the temporal evolution of the density contours for a 5.5 nm particle. **Figure 25 (a)** shows that the nucleation process starts at 97.2 ps and is completed by 108.9 ps for a perfect particle. In case of a void of size 0.98 nm^3, nucleation starts simultaneously at the surface and void at 92.1 ps. The phase change spreads slowly to the rest of the particle and the particle melts by 107.1 ps as seen in **Fig. 25 (b)**. A void size of 8.2 nm^3 shown in **Fig. 25 (c)** is too big for a structurally stable nanoparticle and it starts collapsing at 76.5 ps.

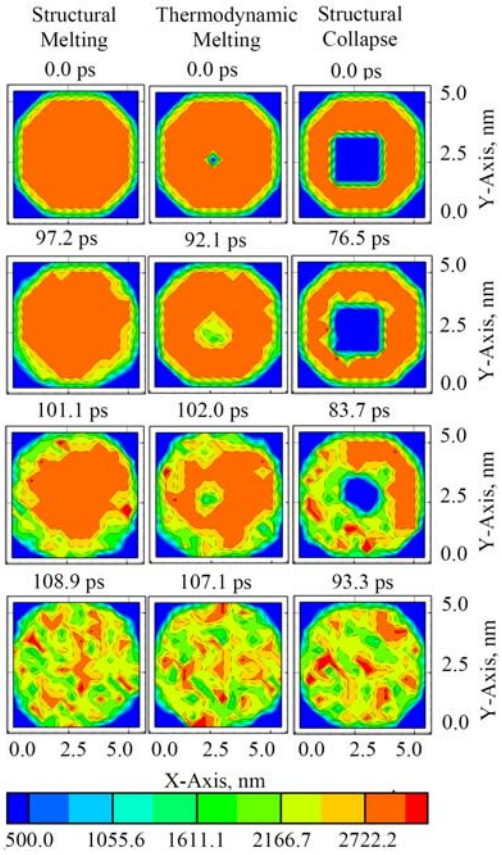

Figure 25. Temporal evolution of density contours, showing mechanism of melting for a 5.5 nm nano particle.

Five different potentials were implemented in the present MD study. Their ensuing results were compared against the cohesive energies of bulk aluminum in the solid state. **Figure 26** shows the results using isobaric-isoenthalpic ensembles. The melting temperature increases from 473 K for a 2 nm particle and reaches the bulk value of 937 K for 8 nm and larger-sized particles. Annealing was accomplished with the velocity scaling at a rate of 0.01 K per step**.**

The two-body Lennard-Jones potential failed to predict the melting point for nano-scale aluminum particles. The Sutton-Chen potential was found to predict geometrical structures for nano clusters very accurately, but failed to provide an accurate prediction of the melting point for nano-scale aluminum particles. The Glue and Streitz-Mintmire potentials are comparable. The former generally leads to a melting temperature about 50-100 K higher than the latter does. The success of the Glue and Streitz-Mintmire potentials in capturing the effect of size on melting of nano particles once again underlines the importance of many-body potentials for modeling aluminum behavior.

The Glue and Streitz-Mintmire potential predict bulk melting points of 1244 K and 1146 K, respectively, which are greater than the thermodynamic melting point by about 18%.

According to the study by Lutsko et al. [7], a factor should be introduced between the simulated (structural) and actual (thermodynamic) melting points when periodic boundary conditions are enforced for bulk materials. The thermodynamic melting point is approximately 0.75-0.85 times its structural counterpart. Application of this factor to the predicted thermodynamic melting point gives a value close to 940 K for bulk aluminum. Since, in the case of particles, the free surface acts as a nucleation site for melting, the phase change predicted by NPH simulations directly corresponds to the thermodynamic melting and no correction factor is required.

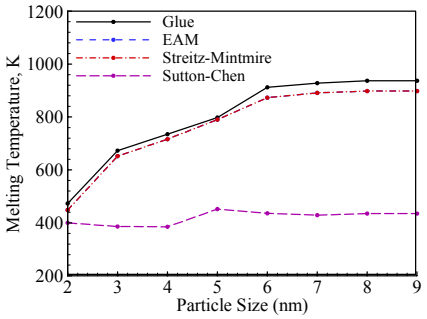

Figure 26. Melting point of nano-scale aluminum particle as function of particle size.

For particles containing 500 atoms or less, uncertainties arise in characterizing the phase transition due to the co-existence of the solid and liquid phases. An alternative approach to obtaining the melting point is thus implemented by equilibrating the particle at specific temperatures and calculating the thermodynamic and structural properties for each respective state. Melting is characterized by fluctuations in the potential energy, a phenomenon referred to as dynamic melting. The particle oscillates between the liquid and solid phases in the temperature range of 450-475 K, as evidenced by the fluctuations in potential energy.

The effect of surface charges on the melting of a nanoparticle also needs to be investigated, although this phenomenon is often negligible for a bulk material due to the lack of surface. The development of surface charges for 2-9 nm particles appears to be too small to exert a significant influence on melting. For particles smaller than 3 nm, the surface charge development plays a negligible role in determining the dynamic melting behavior as well.

From the studies on the melting of a nano-aluminum particle by the **Yang group**, the following key findings have been made.

1. Melting of bulk aluminum is characterized by sharp increases in structural and thermodynamic properties, in contrast to the surface pre-melting for the particulate phase.
2. A perfect crystal features structural melting which is greater than the thermodynamic melting point.
3. Structural melting for aluminum occurs at a temperature of 1244 K. The ratio between the structural and thermodynamic melting points ($f = T_s/T_m$) is 1.32 for aluminum.
4. The range of critical void size increases as the number of atoms considered to represent the bulk phase increases. Increasing the void size beyond a critical value results in collapse of the crystal. The critical value depends on the number of atoms considered in the simulation of the pure crystal.
5. Irrespective of the particle size, the effect of defect nucleated melting is negligible for nano particles because of the presence of surface which acts as a nucleation site.
6. The primary mechanism of melting is nucleation at a surface or void. Phenomena like generation of dislocation were observed in the current study but their impact is negligible compared to nucleation, which is the main mechanism of melting.
7. Melting temperature is independent of the shape and type of void, which is fully consistent with previous studies.
8. The effect of pressure on the defect nucleated melting of aluminum is found to be negligible for pressures up to 300 atm.

9. Five different potentials were implemented. The two-body Lennard-Jones potential failed to predict accurately the melting point for nano particles. The Sutton-Chen potential, validated against structural properties, also led to erroneous results of the melting phenomenon. The Glue and Streitz-Mintmire potentials predicted accurately the size dependence of the melting temperature, but the former generally yielded a melting temperature about 50-100 K higher than the latter.
10. The melting temperature of an aluminum particle increases monotonically from 473 K at 2 nm to the bulk value of 937 K at approximately 8 nm. As the size decreases below a critical value, the increased surface-to-volume ratio and associated higher surface energy enhanced vibrational instability. This interface-induced disorder is responsible for the size dependence of particles melting at nano scales.
11. For particle sizes less than 3 nm, the solid and liquid phases were found to coexist. The effect of surface charge development on melting was explored by analyzing the results from the embedded-atom and Streitz-Mintmire potentials. The Glue and Streitz-Mintmire potentials are identical except that the former completely ignores the electrostatic part of the latter.
12. The development of surface charges has negligible effect on the particle melting characteristics.

Experimental Characterization and Diagnostics

Dlott and his group are studying fundamental mechanisms of the reactive behavior of energetic materials containing nanoparticles using new methods specifically developed to probe events on short time scales and at small length scales. Materials engineering and science is used to create nanoenergetic materials with well-understood structural elements in order to deduce the relationships between these structural elements and performance. By interfacing with researchers who synthesize and engineer new nanomaterials and theorists who study mechanisms of nanoenergetic combustion, bottom-up methods of creating nanoenergetic materials for DoD applications will be developed.

Ultrafast Diagnostics of Nano Energetic Materials

The **Dlott group** has been developing and applying ultrafast diagnostics in their studies of nano energetic materials. The research makes use of:

- Ultrafast infrared spectroscopy combined with laser flash-heating (**Fig. 27**) to study molecular mechanisms of chemistry and nanoscale transport,
- Ultrafast emission spectroscopy to study reactions of metals with oxidizers and to study the time scales of energy release,
- Time-resolved nonlinear or multidimensional spectroscopies to understand heat transfer over short distance scales of a monolayer or nanoparticle, and
- Ultrafast microscopy to characterize the explosive behavior of nanogram or microgram quantities of prototype materials.

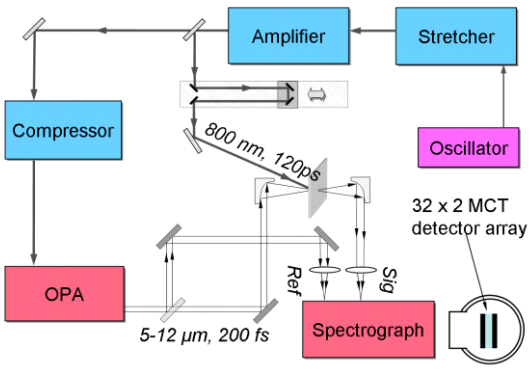

Figure 27. Block diagram of flash-heating laser with two-channel IR detection.

Progress has been made in two general areas. An experimental system that acquires emission spectra with spectral and 30 ps time resolution has been developed. This system has been used to study reactions of Al nanoparticles with nitrocellulose and Teflon. Secondly, an experimental system has been developed that uses femtosecond IR pulses and a new IR array detector to study chemical reactions in real time. This system has been used to study reactions of Al nanoparticles with Teflon. An example of the IR spectra of a nanoenergetic material with 16% nAl with Telfon^{AF} after flash heating with a 0.1 ns pulse is shown in **Fig. 28**.

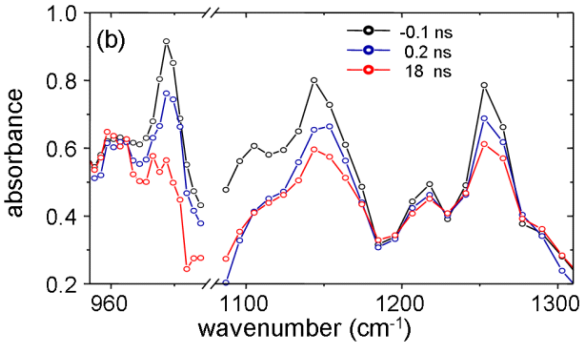

Figure 28. IR spectra of a nanoenergetic material 16% Al (30 nm) with Teflon^{AF} after flash-heating with a 0.1 ns pulse.

During the last year, the group had a lot of problems making nanoparticle fuel/oxidizer samples at the very high densities and compactions needed for these experiments. A little bit of space between nanoparticle and the reaction will not propagate at theoretically maximum rates. We are starting to have success using high pressure/high temperature compaction. Also, new finely granulated nanoparticles with both fuels and oxidizers are becoming available to us from collaborators.

The specific accomplishments during this reporting period have included:

- Ultrafast IR monitoring of chemistry between fuel nanoparticles and oxidizer.
- Time resolved IR and emission of flash-heated energetic material (EM).
- Energy transfer in EM.

In particular, a detailed study of reactions between Al nanoparticles and Teflon^{AF} oxidizer has been completed. Teflon^{AF} has both CF_2 and CFO moieties, and the different rates of reaction of both species can be seen because they are distinguishable in the IR spectrum. The problems the group was having with the emission spectroscopy have been overcome and reliable emission measurements of energetic processes in Al/Teflon^{AF} have been obtained. The dynamics of self-assembled monolayers attached to metal surfaces, which were flash-heated by a laser, have been studied using nonlinear coherent vibrational spectroscopy. A new pulse sequence has been discovered, which eliminates the nonresonant background due to the metallic component.

The **Yetter group** has been developing and conducting research in four areas: flame propagation across the surface and through packed layers of nano aluminum particles, the reaction of quasi-homogeneous mixtures of nAl and gaseous and liquid oxidizers, the reaction propagation and analysis of metastable intermolecular composites (MICs, also referred to as nano thermites) in narrow channels and tubes, and the electrostatic self-assembly of thermite microspheres from nano aluminum and nano copper oxide particles, which was described earlier in this report. A collaborative effort with the **Allara group** on the reactivity of Al-SAM-CuO and Al-SAM-Ni films has been initiated this past year. The **Yetter group** is also beginning to evaluate the combustion characteristics of the nano boron particles fabricated by the **Nuzzo** and **Girolami groups**.

Effect of Added Al_2O_3 on the Propagation Behavior of an Al/CuO Nano-Scale Thermite

One aspect of nano thermite materials that is not well understood is the mode by which energy is transferred ahead of the reaction front to sustain the propagation, or the propagation mechanism. Several propagation mechanisms may be considered when examining the reaction propagation: radiation, conduction, acoustics, compaction, and convection [8]. Solid energetic materials are controlled by conduction, when deflagrating, which can be enhanced by radiation [9,10]. Acoustics (shock processes) and compaction become important when a reaction produces pressures sufficient to induce volume changes in the material. This occurs during detonation or the transition to detonation. Convection is possible if the material is porous and hot interstitial gas, reactants, or products can be propelled forward through the material by high reaction zone pressures [11,12]. Nano-scale thermites exhibit combustion velocities (~1000 m/s) approximately four orders of magnitude greater than that of the micron-scale thermites (~0.1 m/s) [13,14]. The drastic increase in velocity is due to the extremely small time scales associated with mass diffusion and reaction rates brought about by the small particle sizes. This does not allow time for any heat loss or depressurization within the reaction zone leading to high pressure, hot gases that can be propelled ahead of the front. Therefore, these systems are thought to be controlled by a convective propagation mechanism [8].

Because the controlling propagation mechanism is convection, both gas production and temperature, should be important factors when optimizing for the fastest burning rate. Sanders *et al.* [15] observed that for four different metal oxides (Bi_2O_3, MoO_3, CuO, and WO_3), the burning rate on a burn tray was maximized for the mixture ratio that also produced the highest peak pressure in the pressure cell. Moreover, equilibrium calculations showed that all of the optimum stoichiometric ratios were related to the gas production and phase of the products. This optimum stoichiometry was found to be fuel-rich (~1.4) for all of the metal oxides except copper oxide, which optimized at an equivalence ratio close to 1. This difference was attributed to the fact that one of the main products, copper, has a relatively high boiling point of 2835 K and needed the high temperature of a stoichiometric reaction to keep it in the gas phase. Similar to varying the stoichiometry, adding a diluent into the system will decrease the overall temperature of the reaction. Adding the end product as a diluent, particularly Al_2O_3, was a common practice in micron-scale thermite SHS in order to reduce combustion temperatures and change the mechanical properties of the products [16,17]. Moreover, the decrease in combustion temperature gave way to slower reaction velocities and decreasing amounts of gaseous species [14].

In the present work, the effects of dilution by alumina nano-particles on the combustion properties of the Al/CuO nano-scale thermite were investigated. Three types of experiments were performed: the constant volume pressure cell, the unconfined burn tray, and the instrumented burn tube. The nAl had a nominal particle size of 80 nm with 88% active aluminum and the copper oxide particles were assumed to have cylindrical geometry with dimensions of 21 nm × 100 nm. Mixing of reactants was achieved by sonication of the reactants in hexane. Examination of the dried mixture with SEM and TEM indicated that inhomogeneities remained in the mixedness of the reactants, emphasizing the importance of the self-assembly techniques described above. The results showed that the addition of Al_2O_3 decreased the pressure output and reaction velocity in all three experiments. Burn tube measurements showed three reaction velocity regimes (**Fig. 29**): constant velocity observed when 0% (633 m/s) and 5% (570 m/s) of the total weight is Al_2O_3, constant acceleration observed at 10% (146 m/s to 544 m/s over a distance of 6 cm) and 15% (69 m/s to 112 m/s over a distance of 6 cm) Al_2O_3, and an unstable, spinning spiraling combustion wave at 20% Al_2O_3. The pressure measurements correlated to these three

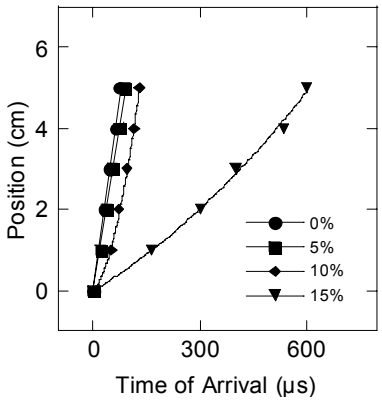

Figure 29. Typical position versus time graphs for reaction waves in the burn tube with various weight percentages of Al_2O_3.

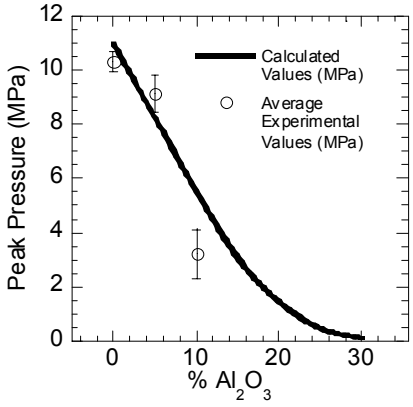

Figure 30. Comparison of average experimental peak pressure values in the burn tube to the calculations for the peak pressure with added Al_2O_3 percentage for constant volume explosion.

regimes showing a drop-off in peak pressure as Al_2O_3 was added to the system, with relatively no pressure increase observed when 20% of the total weight was Al_2O_3. Equilibrium calculations showed that the addition of Al_2O_3 to an Al/CuO mixture lowered the flame temperature, reducing the amount of combustion products in the gas phase, thus, hindering the presumed primary mechanism mode of forward heat transfer, convection. The measured pressure at the flame front was in agreement with equilibrium calculations when a constant volume reaction was assumed (**Fig. 30)**.

Dependence of the Combustion Velocity on Particle Size and Pressure for an Al/CuO Thermite

In order to further understand the propagation mechanism for the Al/CuO nanoscale system, experiments were conducted as a function of initial pressure and for variations in the sizes of the aluminum and CuO particles. In one set of experiments, the sizes of the metal and metal oxide particles were varied between the nanometer and micron scale and the combustion velocities were compared. The results of these experiments indicated that the increased propagation speed of the nAl-nCuO thermite relative to the micron-sized thermite is significantly more sensitive to the CuO particle size rather than the Al particle size. In another set of experiments, the combustion of the nanothermite was examined at various pressures in an argon atmosphere. The results of these experiments revealed an increase in propagation speed when increasing the ambient pressure from 100 to 180 psig, followed by a significant drop-off in propagation speed at higher pressures (**Fig. 31**). At atmospheric pressure in air, the propagation speed was approximately 900 m/s. The trends appear to result from a trade-off between increasing temperature and decreasing gas-pressure at the reaction front with the increase in system pressure. These results are generally consistent with the behavior of micron-sized thermites [14], although the propagation speeds are considerably higher.

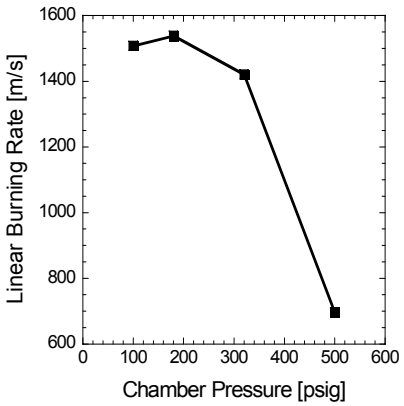

Figure 31. Linear burning rate versus chamber pressure for nanoscale Al/CuO.

Combustion Characteristics of Nanoaluminum, Liquid Water, and Hydrogen Peroxide Mixtures

An experimental investigation into the combustion characteristics of nanoaluminum (nAl), liquid water ($H_2O(l)$), and hydrogen peroxide (H_2O_2) mixtures was also conducted during the last year. Mixtures of nAl with liquid oxidizers represent simple two component systems where the homogeneity of the mixture is easier to control. Steady-state burning rates were obtained at room temperature using a windowed pressure vessel over an initial pressure range of 0.24 to 12.4 MPa in an argon atmosphere, using average nAl particle diameters of 38 nm, ϕ from 0.5 to 1.3, and H_2O_2 concentrations between 0 and 32% by mass. At a nominal pressure of 3.65 MPa, under stoichiometric conditions, mass-burning rates per unit area ranged between 6.93 g/cm^2-s (0% H_2O_2) and 37.04 g/cm^2-s (32% H_2O_2), which corresponded to linear burning rates of 9.58 and 58.2 cm/s, respectively. An example of the deflagration process is illustrated in **Fig. 32**. The effect of H_2O_2 on the burning rates is shown in **Fig. 33** Burning rate pressure exponents at room temperature of 0.44 and 0.38 were found for stoichiometric mixtures containing 10% and 25% H_2O_2, respectively, up to 5 MPa. Burning rates are reduced above ~5 MPa due to voids in the reactant mixture filled with argon gas. Mass burning rates were not measured above ~32% H_2O_2 due to an anomalous burning phenomena, which caused an over-pressurization within the quartz sample holder leading to tube rupture. High-speed videography displayed fingering or jetting ahead of the normal flame front. Localized pressure measurements were taken along the sample length, determining that the combustion process proceeded as a normal deflagration prior to tube rupture, without significant pressure buildup within the tube. In addition to burning rates, chemical efficiencies of the combustion reaction were determined to be within approximately 10% of theoretical maximum at all conditions studied.

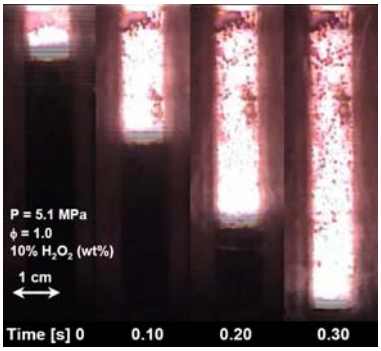

Figure 32. Captured images of the normal deflagration process of a nAl-H_2O-H_2O_2 mixture.

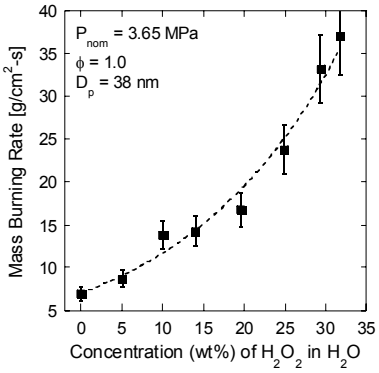

Figure 33. Effect of H_2O_2 concentration on the mass burning rate per unit area of nAl/H_2O mixtures.

Deflagrations of Nitromethane and Nanoaluminum Mixtures

Similar to the studies in which nAl was mixed with H_2O and H_2O_2, the effects of aluminum nanoparticle addition to nitromethane (NM) were also studied in terms of overall mixture burning rate using an optical pressure vessel up to 14.2 MPa. Nitromethane was gelled using fumed silica (Cab-O-Sil), as well as by the nanoaluminum (nAl) particles themselves. Use of the nanoscale metallic particles slightly increased burning rates compared to larger diameter particles, however distinct increases in burning rates were found when Cab-O-Sil was removed and replaced with more energetic aluminum nanoparticles, whose high surface area allowed them to act as the gallant (**Fig. 34**). Burning rates of 2.34 cm/s were seen at 14.1 MPa and 12.5% aluminum loading using 38-nm particles. Using the same nAl particles, 4% aluminum and 3% Cab-O-Sil loading, burning rates of 0.88 cm/s were obtained at approximately the same pressure.

In both cases, mixture consistencies were roughly the same. Larger, 80-nm aluminum particles were also used in conjunction with Cab-O-Sil gellant, yielding a linear burning rate of 0.65 cm/s at 14.2 MPa (4% Al-3% Cab-O-Sil). In all mixtures, burning rate pressure exponents less than the pure nitromethane case were observed with fumed silica addition, while the exponents were increased when using nAl as the gellant.

In addition to the studies described above, the **Yetter group** has received nano boron particles fabricated by the **Nuzzo** and **Girolami** groups at UIUC. The combustion of these particles will be studied in nano thermite and liquid oxidizer mixtures and compared to the nAl studies. The **Yetter group** is also collaborating the **Allara's group** on the reactivity of thin films of Al and CuO and Al and Ni with supporting self-assembled monolayers (SAMs) in between. These experiments will essentially examine the reactivity of the surfaces of the nanoparticles in the microspheres in greater detail.

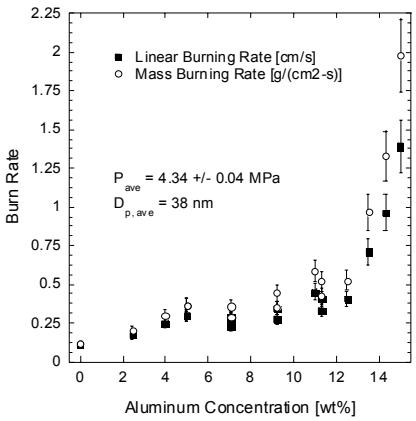

Figure 34. Linear and mass burning rates of mixtures of 38-nm aluminum particles and nitromethane as a function of aluminum loading.

Technology Transfer and Interactions

As discussed throughout the report, the team has developed strong interactions among themselves. In addition, all team members have had close working relationships with various DoD and DoE laboratories. Several collaborative programs with scientists and engineers at ARL, ARDEC, NAVSEA-IH, and LANL have continued to grow.

At Penn State, **Yetter** has continued collaborating with personnel (**Dr. Tim Foley**, **Dr. Bryce Tappan**, and **Dr. Blaine Asay**) at LANL. This past summer, graduate student **Yoni Malchi** spent time with **Dr. Tim Foley** at LANL on the combustion of nanothermites and self assembly of nanoparticles. Since assuming a position at Purdue University after his sabbatical leave at Penn State, **Yetter** and **Yang** have continued to collaborate with **Dr. Son.** This collaboration has resulted in the publication of a special section in the *Journal of Propulsion and Power* on Nano Composite Energetic Materials, the three of whom acted as co-editors. Also contributing to this issue was **Vashishta**, **Kalia**, and **Nakano** at USC in collaboration with **Dr. Barrie Homan** and **Dr. Kevin McNesby** of the Army Research Laboratory. **Allara** and **Yetter** have initiated a joint collaboration on reactive metallic films with SAMs.

Kuo and his team members communicated with **Dr. Jeff Morris** of the Army Research Lab about solubility measurements. **Dr. Morris** was also very helpful in explaining how his solubility tests were set up and executed. His familiarity with carbon dioxide and RDX solutions at elevated pressures was very beneficial in determining the initial set of operating pressure and temperature ranges for the PSU's ultra-high pressure RESS system. **Dr. Morris** also directed the team to previous research studies on RESS systems and several recent work on the theoretical modeling of RDX solubility. The PSU team also discussed with **Mr. Victor Stepanov** of ARDEC of U.S. Army about the particle recovery system. Productive communications were made on this aspect. **Dr. Richard Beyer** of Army Research Lab was also very helpful in supplying two sapphire windows used in this study for recording the dissolution phenomena of RDX in supercritical CO_2.

The **USC group** is collaborating with **Dr. Brad Forch**, **Dr. Barrie Homan**, **Dr. Shashi Karna**, **Dr. Kevin McNesby**, **Dr. Betsy Rice**, and **Dr. Margaret Hurley** at the Army Research Laboratory on energetic materials research. One of their Ph.D. students, Richard Clark, did an internship with **Drs. Hurley** and **Rice** at the Weapons and Materials Directorate in the Propulsion Science Branch, of which **Dr. Forch** is the Chief. **Drs. Forch** and **McNesby** have visited USC to further evolve interactions/collaborations. As mentioned above, the **USC group** has recently published a paper with **Drs. Homan** and **McNesby** at the Army Research Laboratory in the Journal of Propulsion and Power on joint simulation-experimental research of nano-energetic materials.

At UIUC, **Dlott** has discussed his research extensively with collaborators at the DOE labs **LAN, LLNL,** and **Argonne. Dlott** has also had discussions on the mechanisms of reaction propagation in nanoparticles with **Dr. Michelle Pantoya** of Texas Tech U. He has also discussed simulations of nanoparticle combustion with **Vashishta** at USC and Goddard at Caltech, simulations of self-assembled monolayers with **Vashishta** at USC, and spectroscopy of fluorocarbon-coated nanoparticles with **Dr. Jason Jouet** of NSWC. The boron nano particles produced by **Nuzzo** and **Girolami** have been sent to **Yetter** for detailed combustion studies.

List of Papers Submitted or Published under ARO Sponsorship during this Reporting Period

Manuscripts submitted, but not published

1. Alexei Lagutchev, Selezion A. Hambir and Dana D. Dlott, "Nonresonant Background Suppression in Broadband Vibrational Sum-Frequency Generation Spectroscopy", *J. Phys. Chem. C.*, submitted July 2007.
2. Zhaohui Wang, David G. Cahill, Jeffrey A. Carter, Yee Kan Koh, Alexei Lagutchev, Nak-Hyun Seong and Dana D. Dlott, "Ultrafast dynamics of heat flow across molecules", *Chemical Physics*, submitted July 2007.
3. Andrew C. Cortopassi, Kenneth K. Kuo, Peter J. Ferrara, Timothy M. Wawiernia, Jonathan T. Essel, "Synthesis of Nano-Sized RDX Using an Ultra-High-Pressure RESS System," Energetic Material Synthesis and Combustion Characterization for Chemical Propulsion, Begall House Book, submitted for review, 2007.
4. Wontae Noh, Ralph G. Nuzzo, and Gregory S. Girolami, "Boron Nanoparticles from the Pyrolysis of Decaborane," submitted.
5. Charles Spicer, Ralph G. Nuzzo, and Gregory S. Girolami "Chemical Routes to the Synthesis of Energetic Nanomaterials," in preparation.
6. Puri, P. and Yang, V., "Molecular Dynamics Study of Defect Nucleated Melting for Bulk and Nano-Particulate Aluminum," *Journal of Chemical Physics*, submitted 2007
7. Malchi, J.Y., Foley, T.J., and Son, S. F., The Effect of Al_2O_3 Nano-Particles on an Al-CuO Nano-scale Thermite, *Combustion Science and Technology*, submitted 2006.
8. Risha, G. A., Sabourin, J.L., R.A. Yetter, Son, S. F., Tappan, B. C., and Yang, V., nAl-Liquid Water Combustion and Conversion Efficiency, *Combustion Science and Technology*, submitted 2007.
9. J.L. Sabourin, G.A. Risha, R.A. Yetter, S.F. Son, and B.C. Tappan, Combustion Characteristics of Nanoaluminum, Liquid Water, and Hydrogen Peroxide Mixtures, *Combustion and Flame*, submitted 2007.

Papers published in peer-reviewed journals

1. "K. Nomura, R. K. Kalia, A. Nakano, P. Vashishta, A. C. T. van Duin, and W. A. Goddard III, "Dynamic transition in the shock structure of an energetic crystal," *Physical Review Letters*, 2007, in press.
2. P. Vashishta, R. K. Kalia, A. Nakano, B. E. Homan, and K. L. McNesby, "Multimillion atom reactive simulations of nanostructured energetic materials," *Journal of Propulsion and Power* 23, 688-692 (2007).
3. N. Umezawa, R. K. Kalia, A. Nakano, P. Vashishta, and F. Shimojo, "1,3,5-trinitro-1,3,5-triazine decomposition and chemisorption on Al(111) surface: first-principles molecular dynamics study," *Journal of Chemical Physics* 126, 234702: 1-7 (2007).
4. A. Nakano, R. K. Kalia, K. Nomura, A. Sharma, P. Vashishta, F. Shimojo, A. C. T. van Duin, W. A. Goddard, III, R. Biswas, and D. Srivastava, "A divide-and-conquer/cellular-decomposition framework for million-to-billion atom simulations of chemical reactions," *Computational Materials Science* 38, 642-652 (2007).
5. A. Nakano, R. K. Kalia, K. Nomura, A. Sharma, P. Vashishta, F. Shimojo, A. C. T. van Duin, W. A. Goddard, III, R. Biswas, D. Srivastava, and L. H. Yang, "De novo ultrascale atomistic simulations on high-end parallel supercomputers," *International Journal of High Performance Computing Applications,* 2007, in press.
6. "A scalable parallel algorithm for large-scale reactive force-field molecular dynamics simulations," K. Nomura, R. K. Kalia, A. Nakano, and P. Vashishta, *Computer Physics Communications*, 2007, in press.
7. Hyunung Yu, Selezion A. Hambir and Dana D. Dlott, (invited) "Ultrafast dynamics of nanotechnology energetic materials", in Multifunctional Energetic Materials, *MRS Symp. Proc.*; Vol. 896, edited by R. W. Armstrong, N. N. Thadhani, W. H. Wilson, A. Gash, and Z. Munir (2006), Article H03, 9 pages.
8. Hyunung Yu, Dana D. Dlott, F. Richard Kearney, (feature cover article) "Time-resolved microscopy analysis of laser photothermal imaging media", *J. Imag. Sci. Tech*. 50, pp. 401-410 (2006).
9. Dana D. Dlott, Selezion A. Hambir, Hyunung Yu, (invited) "Nanotechnology energetic material dynamics studied with nanometer spatial resolution and picosecond temporal resolution", in Advancements in Energetic Materials and Chemical Propulsion, K. K. Kuo and J. DeD. Rivera, eds. (Redding Ct: Begell House, Inc.,), pp. 22-38.
10. Mikhail A. Zamkov, Rusty W. Conner and Dana D. Dlott, "Ultrafast Chemistry of Nanoenergetic Materials Studied by Time-resolved IR Spectroscopy: Aluminum Nanoparticles in Teflon", *J. Phys. Chem. C* 111, 10278-10284 (2007).
11. Kenneth K. Kuo and Juan de Dios Rivera, Eds., Advancements in Energetic Materials and Chemical Propulsion, published by Begell House, Inc, 830 pages, 2007.
12. Puri, P. and Yang, V., "Effect of Particle Size on Melting of Aluminum at Nano Scales," *Journal of Physical Chemistry C,* 2007, in press.
13. Malchi, J.Y., Son, S.F., R. A. Yetter, and G.A. Risha, Nano-Aluminum Flame Spread with Fingering Combustion Instabilities, *Proceedings of the Combustion Institute*, 31, 2617-2624, 2007.
14. G.A. Risha, R.A. Yetter, S.F. Son, V. Yang, and B.C. Tappan, Combustion of Nano-Aluminum and Liquid Water, *Proceedings of the Combustion Institute*, 31, 2029-2036, 2007.
15. S. Son, R.A. Yetter, and V. Yang, Introduction: Nanoscale Composite Energetic Materials, *Journal of Propulsion and Power*, 23, 4, 643-644, 2007.
16. S. F. Son, T. J. Foley, B. Asay, R.A. Yetter, M. H. Wu, and G. A. Risha, Combustion of Nanoscale Al/MoO_3 Thermite in Microchannels, *Journal of Propulsion and Power*, 23, 4, 715-721, 2007.

Papers published in non-peer-reviewed journals or in conference proceedings

1. Molecular Dynamics Study of melting of Nano Aluminum Particles", by P. Puri, and V. Yang, AIAA Paper-2007-1429, presented at 45th AIAA Aerospace Sciences Meeting and Exhibit, January 2007.
2. "Molecular Dynamics Simulations of Effects of Pressure and Void Size on Melting of Aluminum", by P. Puri, and V. Yang, AIAA Paper-2007-5644, presented at 43rd AIAA/ASME/SAE/ASEE Joint Propulsion Conference and Exhibit, July 2007.
3. J.L. Sabourin, G.A. Risha, R.A. Yetter, S.F. Son, and B.C. Tappan, "Combustion of nano-aluminum, hydrogen peroxide, and liquid water mixtures," JANNAF APS-CS-PSHS Joint Meeting, San Diego, CA, December 2006.

Papers presented at meetings, but not published in conference proceedings

1. J. Y. Malchi, R. A. Yetter and T. J. Foley, Electrostatic self-assembly of a nanoscale thermite system into ordered microspheres, Eastern States Section Fall Technical Meeting of the Combustion Institute, University of Virginia, October 21-25, 2007, submitted August 2007.
2. M.R. Weismiller, J.Y. Malchi, R.A. Yetter, and T.J. Foley, Dependence of the Combustion Velocity on Particle Size and Pressure for an Al/CuO Thermite, Eastern States Section Fall Technical Meeting of the Combustion Institute, University of Virginia, October 21-25, 2007, submitted August 2007.
3. J.L. Sabourin, R.A. Yetter, B.W. Asay, G.A. Risha, and S.F. Son, Deflagrations of Nitromethane and Nanoaluminum Mixtures, Eastern States Section Fall Technical Meeting of the Combustion Institute, University of Virginia, October 21-25, 2007, submitted August 2007.
4. Sabourin, J.L., Risha, G.A., and Yetter, R.A, "Combustion Based Hydrogen Production using Nanoaluminum-Water-Hydrogen Peroxide Mixtures," 2006 Penn State Hydrogen Day, The Pennsylvania State University, University Park, PA, November 14, 2006.
5. Andrew C. Cortopassi, Kenneth K. Kuo, Peter J. Ferrara, Timothy M. Wawiernia, Jonathan T. Essel, "Synthesis of Nano-Sized RDX Using an Ultra-High-Pressure RESS System" Accepted for presentation at the 7th International Symposium on Special Topics of Chemical Propulsion, Kyoto, Japan, September 17-21, 2007.

Honors and Awards

D. Dlott was elected to chair-elect of the Topical Group on Shock Compression of Condensed Matter of the American Physical Society.

G. S. Girolami, Departmental Colloquium Lecturer, University of Florida, May 2007.

G. S. Girolami, Chair-elect of the Governing Board, Council for Chemical Research.

G. S. Girolami, Chair-elect of the Inorganic Chemistry Gordon Conference.

R.G. Nuzzo, 2006 Wall Street Journal Technology Innovation Award for "the development of a process for making large-scale, high-performance electronic circuits that can be applied to any surface."

R.G. Nuzzo, Fellow of the American Academy of Arts and Sciences, 2005.

R.G. Nuzzo, Fellow of the AVS, 2007.

R.G. Nuzzo, Fellow of the World Innovation Foundation, 2004.

R.G. Nuzzo, Recipient of the American Chemical Society's Arthur W. Adamson Award for Distinguished Achievement in the Advancement of Surface Chemistry, 2003.

R.G. Nuzzo, Senior Editor of Langmuir.

V. Yang is appointed to the John L. and Genevieve H. McCain Chair in Engineering at Penn State.

V. Yang receives Best Paper Award of AIAA in 2007.
R.A. Yetter receives Distinguished Paper Award from the Combustion Institute in 2006.

Demographic Data

Demographic Data ***for this reporting period:***

- Number of Manuscripts submitted during this reporting period: **9**
- Number of Peer Reviewed Papers submitted during this reporting period: 1**6**
- Number of Non-Peer Reviewed Papers submitted during this reporting period: **3**
- Number of Presented but not Published Papers submitted during this reporting period: **5**

Demographic Data ***for this reporting period/life of this agreement:***

- Number of Scientists Supported by this agreement (decimals are allowed): **36**
- Number of Inventions resulting from this agreement **0**
- Number of PhD(s) awarded as a result of this agreement: **1**
- Number of Bachelor Degrees awarded as a result of this agreement: **3**
- Number of Patents Submitted as a result of this agreement: **0**
- Number of Patents Awarded as a result of this agreement: **0**
- Number of Grad Students supported by this agreement: **9**
- Number of FTE Grad Students supported by this agreement: **7.5**
- Number of Post Doctorates supported by this agreement: **11**
- Number of FTE Post Doctorates supported by this agreement: **3.3**
- Number of Faculty supported by this agreement: **10**
- Number of Other Staff supported by this agreement: **3**
- Number of Undergrads supported by this agreement: **2**
- Number of Master Degrees awarded as a result of this agreement: **1**

References

1. Armstrong, R.W., Coffey, C.S., DeVost, V.F., and Elban W.L. (1990) Crystal Size Dependence for Impact Initiation of Cyclotrimethylenetrinitramine Explosive, J. Appl. Phys. Vol. 68, No. 3, 1 August.
2. Tom, J.W. and Debenedetti P.G. (1991) Particle Formation with Supercritical Fluids- A Review, J. Aerosol Sci., Vol. 22, No. 5, pp. 555-584.
3. Jung, J. and Perrut, M. (2001) Particle Design Using Supercritical Fluids: Literature and Patent Survey, J. Supercritical Fluids, Vol. 20, pp. 179-219.
4. Debenedetti, P.G. (1990) Homogeneous Nucleation in Supercritical Fluids, AIChE Journal, Vol. 36, No. 9. September.
5. Stepanov, V. Krasnoperov, L.N., Elkina, I.B., and Zhang, X. (2005) Production of Nanocrystalline RDX by Rapid Expansion of Supercritical Solutions, Propellants, Explosives, Pyrotechnics, Vol. 30, No. 3.
6. Morris, J.B. (1998) Solubility of RDX in Dense Carbon Dioxide at Temperatures between 303K and 353K, J. Chem. Eng. Data, Vol. 43, No. 2, pp. 269-273.
7. Lutsko, J.F., Wolf, D., Phillpot, S.R., and Yip, S., "Molecular Dynamics study of lattice-defect nucleated melting in metals using an embedded-atom-method potential," Physical Review B., Vol. 40, No. 5, 1989, pp. 2841-2855.
8. Asay, B. W., Son, S. F., Busse, J. R., and Oschwald, D. M. (2004) Ignition characteristics of metastable intermolecular composites. Prop., Exp., Pyro., 29, 4, pp. 216-219.

9. Son, S. F. and Brewster, M. Q. (1995) Radiation augmented combustion of homogeneous solids. Combust. Sci. Technol., 107, 127.
10. Begley, S. M. and Brewster, M. Q. (2007) Radiative properties of MoO3 and Al nanopowders from light-scattering measurements. J. Heat Trans., 05-1167 (in publication)
11. Kuo, K.K., Chen, A. T., Davis, T. R., Convective burning in solid propellant cracks. AIAA Journal, 16, 6, pp. 600-607, 1978.
12. Ershov, A. P., Kupershtokh, A. L., Medvedev, D. A. (2001) Simulation of convective detonation waves in a porous medium by the lattice gas method. Comb., Exp., and Shock Waves, 37, 2, pp. 206-213.
13. Bockmon, B. S., Pantoya, M. L., Son, S. F., Asay, B. W. and Mang, J. T. (2005) Combustion velocities and propagation mechanisms of metastable interstitial composites. J. App. Phy., 98, 064903.
14. Wang, L. L., Munir, Z. A., and Maximov, Y. M. (1993) Thermite reactions: their utilization in the synthesis and processing of materials. J. Mat. Sci., 28, 3693.
15. Sanders, V. E., Asay, B. W., Foley, T. J., Tappan, B. C., Pacheco, A. N., and Son, S. F. (2006) Combustion and reaction propagation of four nanoscale energetic composites. 33rd Int. Pyro. Sem., pp. 113-121.
16. Varma, A., Lerat, J. P. (1992) Combustion synthesis of advanced materials. Chemical Engineering Science, 17, 9-11, pp. 2179-2194.
17. Munir, Z. A., and Anselmi-Tamburini, U. (1989) Self-propagating exothermic reactions: the synthesis of high-temperature materials by combustion. Mat. Sci. Reports, Vol. 3, 7-8, pp. 277-365.